UNIVERZITA PALACKÉHO V OLOMOUCI

PŘÍRODOVĚDECKÁ FAKULTA

KATEDRA OPTIKY

BAKALÁŘSKÁ PRÁCE

Optická zařízení pro kvantové zpracování informace

Vypracovala: Helena Fikerová

Vedoucí práce: Prof. RNDr. Miloslav Dušek, Dr.

Obor: Optika a optoelektronika

Olomouc 2010

Prohlášení

Prohlašuji, že jsem bakalářskou práci vypracovala samostatně pod vedením Doc. RNDr. Miloslava Duška, PhD. a za použití zdrojů uvedených v seznamu použité literatury.

V Olomouci dne 30. července 2010

PALACKY UNIVERSITY OLOMOUC

FACULTY OF SCIENCE

DEPARTMENT OF OPTICS

BACHELOR THESIS

Optical Setups for Quantum Information Processing

Author: Helena Fikerová

Thesis Supervisor: Prof. RNDr. Miloslav Dušek, Dr.

Field of Study: Optics a Optoelectronics

Olomouc 2010

CONTENT

Introduction

The aim of this diploma project was to implement a functional electronic feed-forward control in an interferometric quantum-optical device which would later be used for linear optical quantum information processing. The term feed-forward designates a technique which uses a control signal to modify the output of a system in a predefined way without affecting the subsequent input. It is conveniently being employed as real-time error correction in optical quantum computing where the control signal is produced by measurement on ancilla qubits and applied via fast electro-optical modulators.

The project described in this paper is part of an ongoing larger experiment whose purpose is to build a programmable single-qubit quantum gate that would apply a phase shift to the data qubit according to the phase shift present with an ancilla (program) qubit, similar to [1], but using fiber optics, qubits encoded into spatial modes and feed-forward to increase the probability of success.

The device that we used for testing feed-forward control consists of a source of entangled photon pairs generated by parametric down conversion and a fiber Mach-Zehnder interferometer. To form the quantum gate, the setup will have to be enlarged into two intertwined Mach-Zehnder interferometers.

The first part of the following text explains the motivation for the experiment with which this diploma project is concerned; it outlines basic research intentions and challenges of quantum information processing and optical implementations of information processing tasks. The possibility of achieving quantum computing using linear optics and feed-forward technique is illustrated on the example of a programmable single-qubit phase gate. The ensuing section of the text focuses on key features and basic principles of the Mach-Zehnder interferometer and characteristic aspects of parametric down conversion. The experimental setup, methods and results of the project are described and discussed in the rest of the paper.

1 Linear Optical Quantum Information Processing

The main idea behind Quantum Information Processing (QIP) is the use of quantum mechanics for manipulating information. Nowadays information technology exploits classical physics to store and handle units of information. For decades, while using the same laws of electrodynamics, manufacturers have been succeeding to improve the performance of computers and make them smaller and faster. However, regarding certain problems the efficiency of "classical" computers is largely limited.

The *efficiency* of an algorithm used to solve a problem is determined by the amount of resources a computer spends to run it. The most important computational resources are time and memory space and their amount is measured in terms of the length of input of the problem. If a resource depleted on the algorithm can be expressed as a polynomial or any other slower growing function, the algorithm is considered to be efficient. If the amount of resources needed increases exponentially with the length of input, the algorithm is considered inefficient. [2] It is evident that the quantity of resources necessary for the execution of an information processing task depends on how this task is carried out physically. Therefore different physical computing structures have different efficiencies for different algorithms.

It has been theoretically shown [3] that a computing device availing of quantum mechanical phenomena would be able to solve certain problems, such as the factoring of large numbers [4] or simulations of quantum systems [5], much faster than a classical computer. Though it is theoretically possible to solve these problems on the state-of-the-art computers, in practice the computation is inefficient and would take up a virtually infinite amount of time whereas quantum computation would be exponentially faster.

The exponential advantage over a classical device is made possible by the existence of quantum superposition and entanglement. The basic unit of information in classical computing is the classical bit; a bit is always either in state 0 or 1. The quantum unit of information is the qubit; a qubit, just like an ordinary bit, can be found in two different states, say 0 or 1, but it can in general exist in a superposition of both. It is thus a two-state quantum system which can be represented by a state ket in a two-dimensional Hilbert space spanned by two state kets corresponding to state 0 and 1. We can therefore express the state of a qubit:

$$|\psi\rangle = \alpha|0\rangle + \beta|1\rangle$$

where α and β are complex numbers representing the probability amplitudes, so the probability of finding the qubit in state $|0\rangle$ is $|\alpha|^2$ and the probability of finding it in state $|1\rangle$ is $|\beta|^2$.

The state of a system composed of m qubits is in general a superposition of 2^m base states $|x\rangle$ each one of which is a combination of possible qubit states:

$$|\Psi\rangle = \sum_{x=1}^{2^m} \alpha_x |x\rangle$$

If we consider a register (a device that records data) constructed out of m qubits, each base state $|x\rangle = |a_1, a_2, \dots, a_m\rangle$ of the register can represent a number a via the binary combination

$$a = 2^0 a_1 + 2^1 a_2 + \cdots + 2^{m-1} a_m \,.$$

We may note that for a full description of the state of a classical m-bit register m integers are necessary while the state of a quantum m-bit register is specified by 2^m complex numbers α_x. In other words, in a sense the information storage capacity of quantum registers grows exponentially with the number of units of information in comparison to the classical registers. While a classical m-bit register stores only one of the 2^m numbers, an m-qubit register can keep a record of 2^m numbers at once. In some cases, this might mean an exponential advantage. However, when it is measured, the state of a quantum register collapses to one of its base states and thus gives us information about one of the base states only. [6,7] Nevertheless, if availed of adroitly, quantum superposition can bring about more efficiency thanks to entanglement.

1.1 Optics in Quantum Information Processing

Since a quantum computer was theoretically defined, there have been many different proposals for the physical implementation of a quantum information processing device. Besides efficiency, the major concerns here have been *universality* and *scalability*. A set of logic gates that operate on qubits and evolve their quantum state is called universal if all possible unitary evolutions (that embodies any logic function) can be approximated by a sequence of gates from the set [2, 8]. Similarly, a

quantum gate is universal if a sequence of its copies can approximate any arbitrary unitary evolution. With a quantum computer in mind, on which we would like to perform all sorts of different tasks, it is thus desirable that physical executions of basic quantum processing tasks be universal. Furthermore, efficient quantum computation protocols acting on small volumes of information are not necessarily efficient in a large scale. In order to stay efficient with increasing problem size, the demand of resources has to grow at most in a polynomial fashion. In other words, if a scheme of quantum computation is to be useful it should be scalable.

Among other means of QIP physical implementations that have been thought of optics has the advantage of photons tending to keep the information they carry (they undergo negligible decoherence), so interference is easily seen, and the preparation of entangled states being simple. Photons could thus represent qubits with the base states given by two optical modes. However, photons do not naturally interact with each other which is essential for the operation of logic gates. They can interact directly in nonlinear media, so one possibility would be to construct quantum gates based on nonlinear couplings between photons, but in reality these are difficult to induce at sufficiently large magnitudes. Another possibility is offered by linear optics while introducing indirect interaction through photon measurements with detectors. Because such linear optical gates are probabilistic (their probability of failure is very high), it was believed that to compensate for errors an exponential number of optical modes was needed which clearly could not be scalable [8, 9]. Nevertheless, in 2002 it was shown by Knill, Laflamme and Milburn [8] that efficient and likely scalable universal linear optical quantum information processing was possible with only linear resource requirements.

1.2 The Application of Linear Optics and Feed-forward in QIP

The scheme for optical quantum computation proposed by Knill, Laflamme and Milburn (KLM) in [8] requires but single photons, linear optics and measurement, so that only single photon sources, beam splitters, phase shifters and photon detectors are needed for its physical implementation. As shown by Lloyd [10] most two-qubit gates together with some single-qubit operations are universal in general. The KLM protocol achieves universal quantum computation by means of a conditional sign flip operation between two qubits which is essentially a two-qubit controlled-phase gate constructed out of two nonlinear sign (NS) gates. The NS gates can only be

implemented as probabilistic; with the use of two ancilla qubits measurements and post-selection they have 1/4 probability of success in which case the conditional sign shift succeeds with probability 1/16. Efficiency demands are reached via quantum teleportation and relevant error correction is suggested to convey scalability [8,9]. In this way the KLM scheme proves that universal efficient scalable QIP with linear optics is in principle possible.

There have been many improvements to the KLM architecture since. One of the methods for increasing the success probability of NS and other linear optical gates is provided by the technique of feed-forward which uses classical information from single-photon detectors to modify the output qubit states. Auxiliary measurement of an ancilla photon produces a signal that is fed forward in the quantum circuit and applied via an electro-optical modulator to correct for error caused by the probabilistic aspects of a gate, as showed by [11] on a quantum parity check single-qubit gate increasing the probability of success from ¼ to 1/2.

1.3 Programmable Phase Gate

The programmable phase gate is an example of a linear optical quantum gate whose probability of success can be increased through feed-forward from ¼ to 1/2. This single-qubit gate applies a unitary operation - a phase shift, fully specified by the state of a program qubit - to a data qubit. If we prepare the state of the program qubit as an equal superposition of two basis states corresponding to two modes with a relative phase factor of ϕ between them:

$$|\psi\rangle_{PRG} = \frac{1}{\sqrt{2}}\big(|0\rangle + e^{i\phi}|1\rangle\big),$$

and the data qubit as a general superposition of two possible states:

$$|\psi_{IN}\rangle_{DAT} = \alpha|0\rangle + \beta|1\rangle,$$

the gate introduces a phase shift of ϕ between the basis states of the output data qubit, i.e. rotates the data qubit state by an angle ϕ around the equator of the Bloch sphere:

$$|\psi_{OUT}\rangle_{DAT} = \alpha|0\rangle + e^{i\phi}\beta|1\rangle.$$

A more detailed theoretical picture of the gate can be provided by the following scheme:

1/2(|0⟩+e^{iφ}|1⟩)

$|1⟩_1$

$|0⟩_2$

BS

$|0⟩_1$

$|1⟩_2$

$\alpha|0⟩+\beta|1⟩$
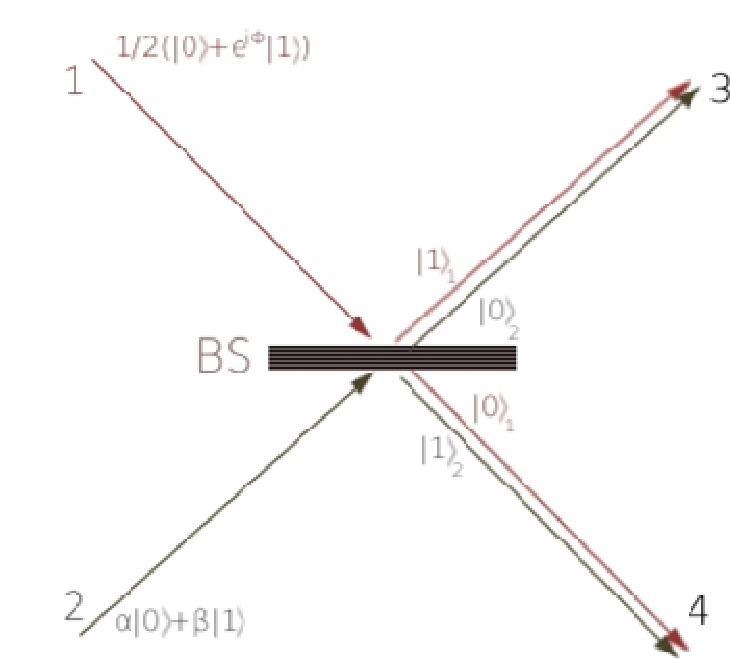
Let's consider a beamsplitter that transmits all states 0 and reflects all states 1 (as indicated on Figure 1). When two qubits $|\psi\rangle_{PRG} = \frac{1}{\sqrt{2}}\left(|0\rangle + e^{i\phi}|1\rangle\right)$, coming from the path labeled 1 and $|\psi_{IN}\rangle_{DAT} = \alpha|0\rangle + \beta|1\rangle$, coming from the path labeled 2, meet at the beamsplitter, the resulting quantum state is equal to

$$|\psi\rangle_{PRG}|\psi_{IN}\rangle_{DAT} = \frac{1}{\sqrt{2}}\left(\alpha|0_1, 0_2\rangle + \alpha e^{i\phi}|1_1, 0_2\rangle + \beta|0_1, 1_2\rangle + \beta e^{i\phi}|1_1, 1_2\rangle\right),$$

where $|0_1, 0_2\rangle$ is a shorthand notation for $|0_1\rangle|0_2\rangle$. Transmission and reflection at the beamsplitter change the state into

$$|\psi_{OUT}\rangle = \frac{1}{\sqrt{2}}\left(\alpha|0_4, 0_3\rangle + \alpha e^{i\phi}|1_3, 0_3\rangle + \beta|0_4, 1_4\rangle + \beta e^{i\phi}|1_3, 1_4\rangle\right),$$

where the states' indices indicate output paths labeled 3 and 4 on Figure 1. A post-selection is made; the cases of two photons in the same path are discarded. The available states are thereupon

$$\frac{1}{\sqrt{2}}\left(\alpha|0_4, 0_3\rangle + \beta e^{i\phi}|1_3, 1_4\rangle\right).$$

Now suppose that two detectors are placed in path 3 as illustrated on Figure 2. If a measurement is performed in the basis

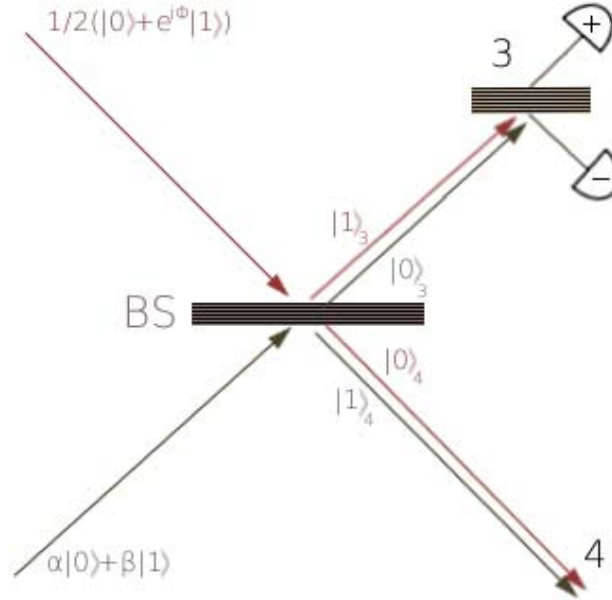$$|\pm\rangle_3 = \frac{1}{\sqrt{2}}(|0_3\rangle \pm |1_3\rangle),$$

$1/2(|0\rangle + e^{i\phi}|1\rangle)$

$|1\rangle_3$

$|0\rangle_3$

BS

$|0\rangle_3$

$|0\rangle_4$

$|1\rangle_4$

$\alpha|0\rangle + \beta|1\rangle$

3

4

Figure 2: Measurement at detector (+) corresponds to the projector
$|+\rangle\langle+|$, measurement at detector (-) corresponds to the projector $|-\rangle\langle-|$.

with the detector labeled (+) projecting $|\psi_{OUT}\rangle$ onto $|+\rangle$ and the detector labeled (−) projecting $|\psi_{OUT}\rangle$ onto $|-\rangle$, it yields the state

$$|\pm\rangle_3\langle\pm|\psi_{OUT}\rangle = |\pm\rangle_3 \frac{1}{2}(\langle0_3| \pm \langle1_3|)(\alpha|0_4, 0_3\rangle + \beta e^{i\phi}|1_3, 1_4\rangle)$$

$$= \frac{1}{2}(\alpha|0_4\rangle \pm \beta e^{i\phi}|1_4\rangle)|\pm\rangle_3$$

Hence there is ¼ probability that detector (+) responds; if it does, it means that we have obtained the desired state $\alpha|0\rangle + \beta e^{i\phi}|1\rangle$ which takes the exit 4. However, if detector (−) fires, the state $\alpha|0\rangle - \beta e^{i\phi}|1\rangle$ is present in path 4 and a phase shift of $\phi + \pi$ instead of ϕ was applied. The unwanted case also has ¼ probability of happening, which can be conveniently reduced to zero via feed-forward control (see Figure 3) thus increasing the probability of success of the gate to ½. Feedback from detector (−) can be taken advantage of to modify the phase between modes 0 and 1 in path 4. If the phase shift of π is administered, we will obtain the right state again. In

other words, every time detector (–) fires, the gate will correct for wrong phase shift by itself when feed-forward control exists between detector (–) and path 4.

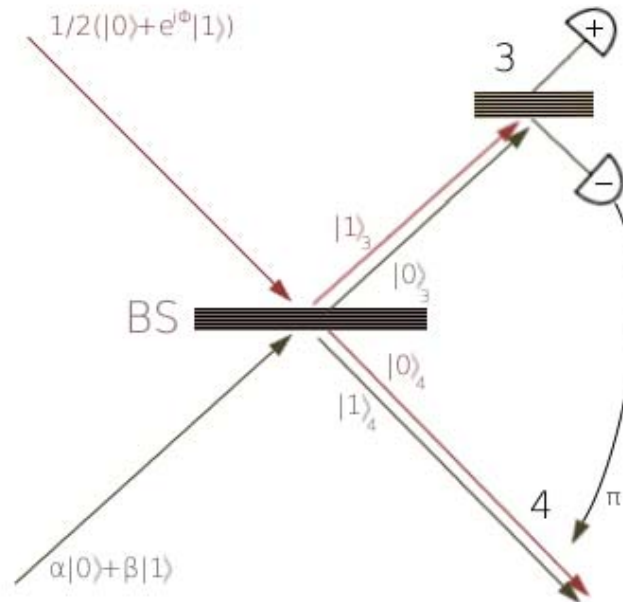
Figure 3: Feed-forward taking advantage of the feedback from detector
– increases the probability of success of the gate from ¼ to ½.

A linear optical implementation of the programmable phase gate was performed in the past with qubits encoded into photons' polarization states [1] but without using feed-forward. The same setup has also been used to perform minimal disturbance measurement [12].

2 Parametric Down-Conversion

From a practical point of view, parametric down-converters are useful entangled photons and single-photon sources because they can be relatively simply implemented. Entangled pairs of ancilla and data qubits in the setup described in this paper and in linear optical gates setups mentioned above [1, 11] were generated via such sources.

Spontaneous parametric down-conversion is a quantum phenomenon occurring in nonlinear crystals such as $LiIO_3$ (used in our setup), BBO (used in [11]) or $KNbO_3$[1] which has its origin in the nonlinear behavior of the crystal medium in applied strong electromagnetic fields. The crystal response, i.e. the dielectric polarization, to strong fields is not directly proportional to the electric field intensity anymore and thus atoms in the crystal lattice behave as anharmonic oscillators. Consequently, some photons interacting with the crystal have a non-zero probability of being converted to two less energetic ones while the crystal medium does not alternate so the condition of total energy and momentum conservation has to hold. The incoming photon frequency thereupon has to be equal to the sum of the generated photon pair frequencies

$$\omega_{in} = \omega_{1out} + \omega_{2out}$$

and directions in which the generated photons will travel have to satisfy the momentum vector equality

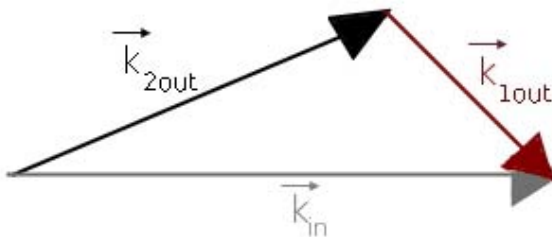$\vec{k}_{in} = \vec{k}_{1out} + \vec{k}_{2out}$ (see Figure 4).

Figure 4: The conversion has to satisfy the condition of momentum conservation.

This implies that the three photons will in general travel in different directions (see Fig. 5) and all possible $\vec{k}$ vectors combinations are equally probable, so the resulting

---

[1] LiIO3 – lithium iodate, BBO – barium beta-borate, $KNbO_3$ – potassium niobate

final state of the outcoming light will be a superposition of possible $\vec{k}$ states. The conversion is triggered by random vacuum fluctuations (it cannot be explained by classical electromagnetic theory); for which reason generated photons pairs will be emitted at random times in two cones on, in general[2], opposite sides of the incoming beam (see example on Fig. 5).
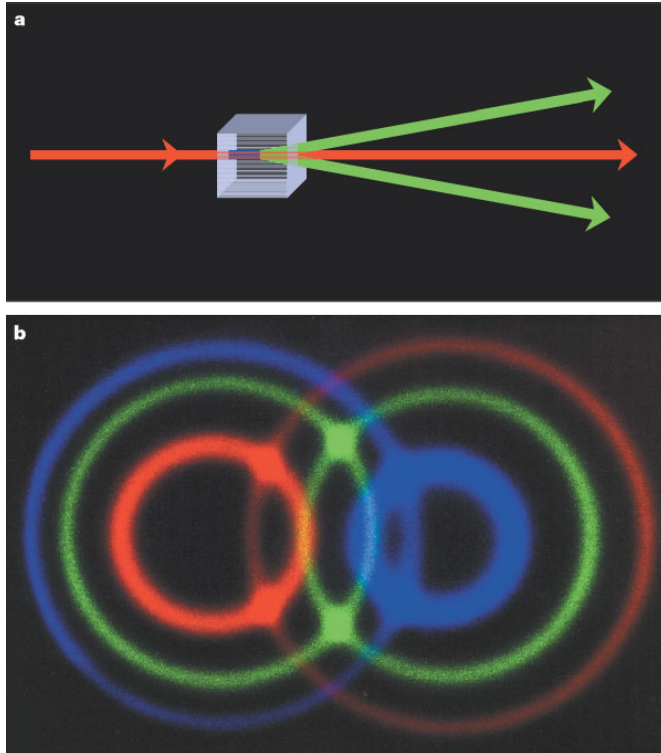
Figure 5: Parametric down-conversion, from C. Monroe, Nature **416**, 238-246(2002).

By placing two apertures after the nonlinear crystal in two directions which satisfy the momentum and frequency conservation condition it is possible to select pairs of photons non-classically correlated (entangled) in frequency (and therefore in energy, too). The twin photons are usually being labeled as signal and idler; the presence of the idler thus indicates simultaneous presence of the signal [6].

---

[2] They might also both lie in the direction of the incoming beam.

3 The Mach-Zehnder Interferometer

The Mach-Zehnder interferometer is a basic interferometric device constituting, in a bulk setup, of two beamsplitters (dielectric mirrors), two mirrors and two detectors. The first beamsplitter divides incoming light into two separate paths which are bended by the two mirrors in order to meet again at the second beamsplitter, where light beams interfere (Fig. 6). Interference fringes can be observed at detectors A and B when the relative phase between photons coming from mirrors M_1 and M_2 is varied.
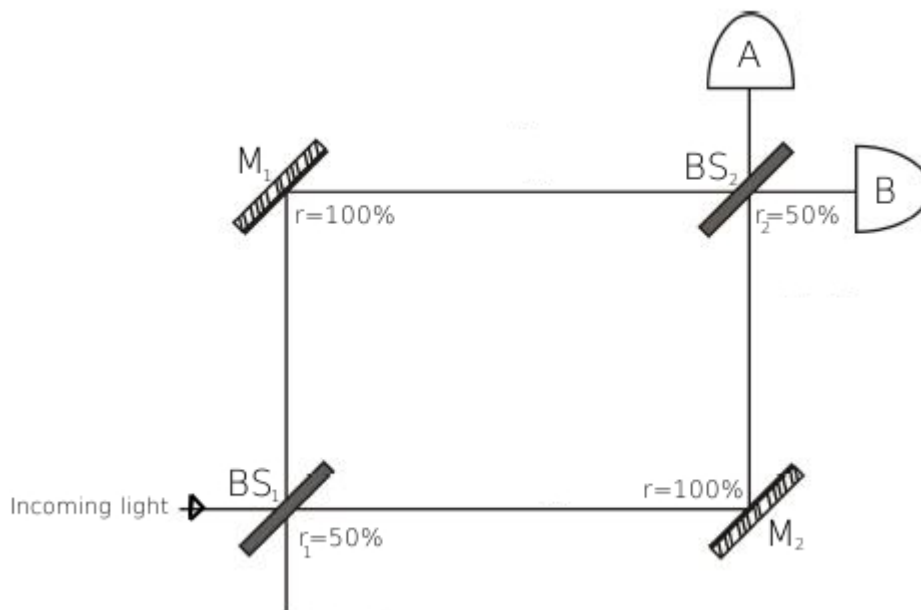
Figure 6: The Mach-Zehnder interferometer; BS – beamsplitter, M – mirror, A,B – detectors.

3.1 Basic Principle

For a better understanding of how interference can be observed, it is useful to look at the general outcome at detectors A and B in the special case of a bulk implementation of a Mach-Zehnder which uses beamsplitters in the form of dielectric mirrors. Let's consider the difference of light paths at the second beamsplitter for detector A and B separately. Reflection on a surface with a refractive index lower than that of the propagation medium causes no phase shift, whereas reflection on a surface with a higher refractive index induces a phase shift of π[3]. Thus light reflected at BS_1

---

[3] Note that this explanation is built upon the special simple case of a transverse wave.

takes up a phase shift of π at BS$_1$, π at mirror M$_1$ and another phase shift of π when reflected towards detector A. When transmitted towards B, it picks up a phase shift of $\frac{2\pi}{\lambda} \cdot d_2$ inside BS$_2$ where d is the optical path length through the beamsplitter medium. If we also consider the path length p_1 which is the distance from BS1 to M1 plus the distance from M1 to BS2, the total phase of light taking this path is:

$$3\pi + \frac{2\pi}{\lambda} p_1 \quad \text{(arriving at A)}$$

and

$$2\pi + \frac{2\pi}{\lambda}(d + p_1) \text{ (arriving at B)}$$

Light transmitted by BS$_1$ picks up a phase shift of $\frac{2\pi}{\lambda} \cdot d$ when going through BS$_1$ (d$_1$ is the optical path length) plus π at mirror M$_2$. In the case of transmission towards A, we have to add a phase shift of $\frac{2\pi}{\lambda} \cdot d$, in the case of reflection towards B, the corresponding phase shift is $2 \cdot \frac{2\pi}{\lambda} \cdot d$ (we suppose that light enters the beamsplitter from its uncoated side, but the positioning is irrelevant to the final result). The total phase shift is therefore:

$$\pi + \frac{2\pi}{\lambda} \cdot 2d + \frac{2\pi}{\lambda} \cdot p_2 \qquad \text{(arriving at A)}$$

and

$$\pi + \frac{2\pi}{\lambda} \cdot 3d + \frac{2\pi}{\lambda} \cdot p_2 \qquad \text{(arriving at B)}$$

Light beams that interfere at BS$_2$ and get detected at A thus have a phase difference of

$$2\pi + \frac{2\pi}{\lambda}(p_1 - p_2) - \frac{2\pi}{\lambda} \cdot 2d = 2\pi + \delta \text{ (detector A),} \qquad (1)$$

whereas light beams that get detected at B have a phase difference of

$$\pi + \frac{2\pi}{\lambda}(p_1 - p_2) - \frac{2\pi}{\lambda} \cdot 2d = \pi + \delta \quad \text{(detector B).}$$

Hence if the phase difference for light going to A is δ than the phase difference for light going to B is $\delta + \pi$. It is clear from the result that every time constructive interference is detected at A, destructive interference can be seen at B and vice versa [6, 13], in accordance with the law of energy conservation.

If the phase difference between light going through the two different paths is varied (if δ is varied), e.g. by changing the difference in path lengths, and intensities at detectors A and B are recorded, time interference fringes will be observed (see Fig.7). The intensity recorded at detector A is then given by the interference equation [14]

$$I^A(t) = I^A_{M_1} + I^A_{M_2} + 2\sqrt{I^A_{M_1} I^A_{M_2}} \cos\delta(t) \qquad (2)$$

where $I^A_{M_1}$ and $I^A_{M_2}$ denote intensities of light waves coming to A by the two different path. The same holds for B though in this case, with respect to the phase difference of π between light arriving at A and B, we may write

$$I^B(t) = I^B_{M_1} + I^B_{M_2} + 2\sqrt{I^B_{M_1} I^B_{M_2}} \sin\delta(t).$$

Therefore

$$I^A_{max}(t) = I^A_{M_1} + I^A_{M_2} + 2\sqrt{I^A_{M_1} I^A_{M_2}}, \qquad (3)$$

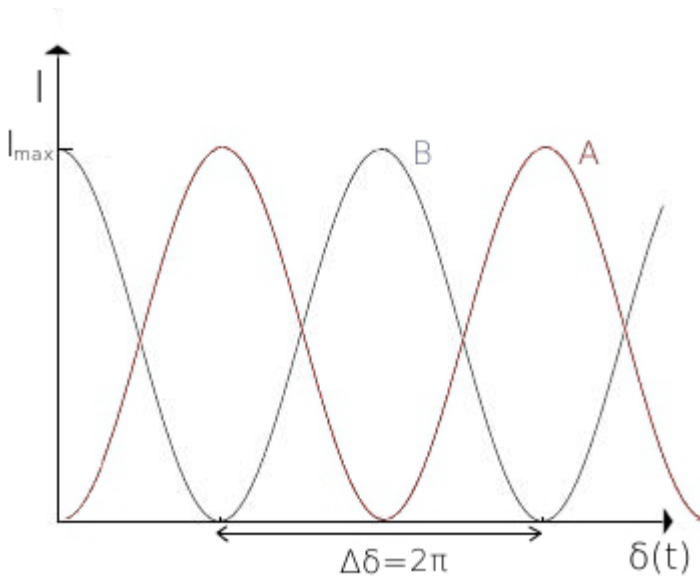$$I^A_{min}(t) = I^A_{M_1} + I^A_{M_2} - 2\sqrt{I^A_{M_1} I^A_{M_2}}. \qquad (4)$$

Figure 7: Time interference fringes observed on the outputs of a Mach-Zender interferometer.

3.2 Interference Contrast

In stating (2) we have supposed the ideal situation of perfectly coherent light. In order to take into account light fluctuations at the point of interference and

correlations of these fluctuations between interfering light waves, the complex degree of temporal coherence $g_{12}(\tau)$ has to be introduced:

$$I^A(\tau) = I^A_{M_1} + I^A_{M_2} + 2\sqrt{I^A_{M_1}I^A_{M_2}}|g_{12}(\tau)|cos\delta(\tau) \quad (5)$$

where $\tau = t_1 - t$.

The value $|g_{12}(\tau)|$ is a measure of the degree of correlation between light amplitudes $U_1(t)$ and $U_2(t + \tau)$ at instances t and t_1 respectively. The degree of coherence $g_{12}(\tau)$ is given by

$$g_{12}(\tau) = \frac{\langle U_1^* U_2 \rangle}{(I^A_{M_1} I^A_{M_2})^{1/2}}$$

where $I^A_{M_1} = |U_1|^2$ and $I^A_{M_2} = |U_2|^2$; and the value of its module lies between zero and one:

$$0 \le |g_{12}(\tau)| \le 1$$

with the value of 0 pertaining to completely incoherent light and the value of 1 to perfectly coherent light.

The "quality" of interference can be measured with the contrast of interference fringes which is specified by *interferometric visibility*, defined as

$$V = \frac{I_{max} - I_{min}}{I_{max} + I_{min}}, \qquad\qquad (6)$$

where I_{max} is the maximum and I_{min} the minimum intensity of a fringe. Visibility is determined by the correlation coefficient. If we rewrite (3) and (4) according to (5), we get:

$$V = \frac{4 \cdot \sqrt{I^A_{M_1} I^A_{M_2}}|g_{12}(\tau)|}{2 \cdot (I^A_{M_1} + I^A_{M_2})} = 2 \cdot \frac{\sqrt{I^A_{M_1} I^A_{M_2}}}{(I^A_{M_1} + I^A_{M_2})} \cdot |g_{12}(\tau)|$$

Thus V is proportional to $|g_{12}(\tau)|$. In the case when $I^A_{M_1} = I^A_{M_2}$, $V = |g_{12}(\tau)|$ [14, 15].

4 Experimental Setup

The constituent parts of the setup we used throughout this project were a single-photon source, a fiber Mach-Zehnder interferometer and single-photon APD (Avalanche Photodiode) detectors. The fiber implementation of the Mach-Zehnder interferometer which uses fiber couplers to divide the incoming beam into two fibers and rejoin them again has the advantages of simple paths adjustment (there is obviously no need of mirrors), precise spatial beam overlap for interference (if single-mode fibers are used) and better mechanical stability in comparison with bulk interferometers. It is very convenient for carrying out feed-forward control, as feedback from detectors which is in the form of TTL pulses can be applied to the setup directly via electro-optical phase modulators, though a voltage divider might be needed to adjust the pulse height. On the other hand, fiber components such as polarizers and fiber connectors suffer from losses that are relatively large when compared to bulk setups constituents, but this is not a fundamental obstacle to our project as long as high interference contrast can be achieved. Another disadvantage lies in the fiber refractive index being sensitive to temperature fluctuations which results in phase drift; however, appropriate thermal isolation of the interferometer and active phase correction should be able to solve the problem.

It was already mentioned above that this thesis was part of a larger project the aim of which is to build a programmable single-qubit quantum gate. The gate has already been implemented using linear optics, bulk optical components and photonic qubits encoded into polarization states [1]; our linear optical scheme employs fiber optics and qubits encoded into spatial modes of photons seeing that it is difficult to control polarization in optical fibers. The fiber Mach-Zehnder interferometer in our setup for feed-forward testing which is supplied by a single-photon source thus represents a qubit

$$|\psi\rangle = \alpha|0\rangle + \beta|1\rangle$$

with the states 0 and 1 corresponding to two spatial modes realized by the two arms of the interferometer and their superposition made possible by single-photon interference. The probabilities $|\alpha|^2$ and $|\beta|^2$ are determined by the relative intensities going through the interferometer arms.

4.1 Setup for Interference Optimization

The fact that the appearance of the fiber version of a Mach-Zehnder interferometer is slightly different to the bulk scheme depicted on Fig. 6 leaves the underlying physics (described in section 3 of this text) unchanged. In the case of an ideal stable Mach-Zehnder interferometer, we should always be able to read zero and maximum intensities (or counts) at the two detector outputs respectively if the phase shift difference δ in (1) is equal to 0. Such a situation would correspond to a visibility $V = 1$. In the real case V is always less than 1 due to error and imperfections of the physical setup, but it can be made close to one if interference optimization through interferometer adjustment is performed. For the sake of our feed-forward demonstration (see Section 4.2) it was necessary to reach high interferometer visibilities so that the interferometer output be as close as possible to the ideal case with $\delta = 0$.

The setup used for interferometer adjustment is depicted on Figure 8 here below (for actual setup appearance see snapshot A1 in Appendix).
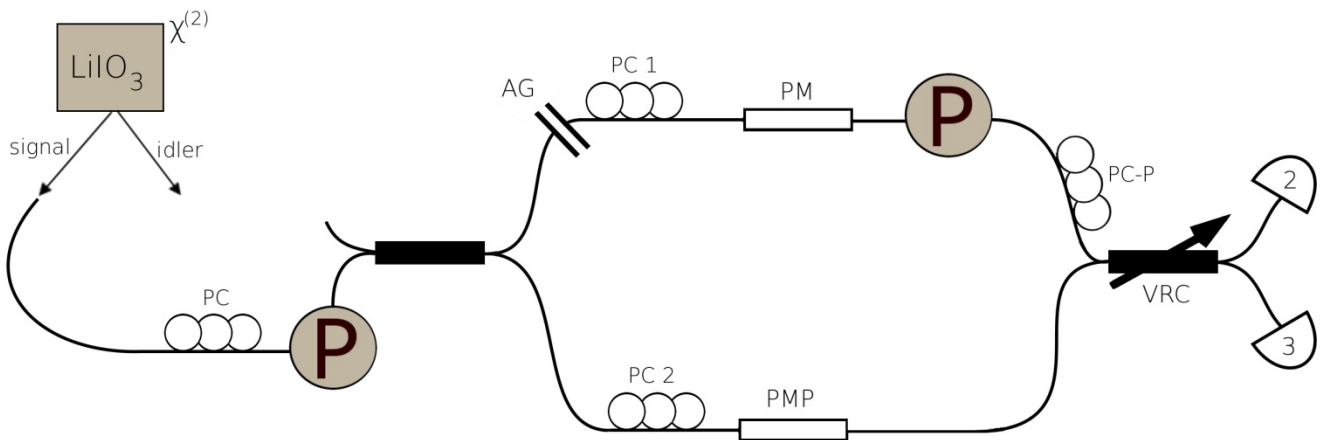
Figure 8: Setup for interferometer adjustment. The fiber Mach-Zehnder interferometer is supplied by signal photons from a parametric down-converter. The following labels stand for: P - polarizer, PC – polarization controllers, AG – adjustable air gap, PM – phase modulator, PMP – phase modulator with an integrated polarizer, VRC – variable ratio coupler, 2,3 – detectors (the APD module used constituted of four detectors labelled 0, 1, 2 and 3).

The source produces entangled photon pairs. The signal photons are coupled into a fiber and conducted into the interferometer where they interfere with themselves at the second variable fiber coupler and get detected at detectors 2 and 3.

4.1.1 Source

The source we used was a nonlinear lithium iodate (LiIO$_3$) crystal pumped by 407nm laser beam. Photon pairs generated by parametric down-conversion, travelling from directions at the same angle with and on opposite sides of the incoming beam axis, were selected with apertures and coupled into fibers (see Figure 9); the wavelength of both idler and signal photons was around 814nm. However, the idler part of the photon pair was not needed until the setup had to be adjusted for feed-forward control implementation; that is why it is depicted as left idle on the setup scheme on Fig. 8.

The laser used was a 50mW Cube 1069413 from Coherent (Serial # 99867301); we had it operating at 40mW.
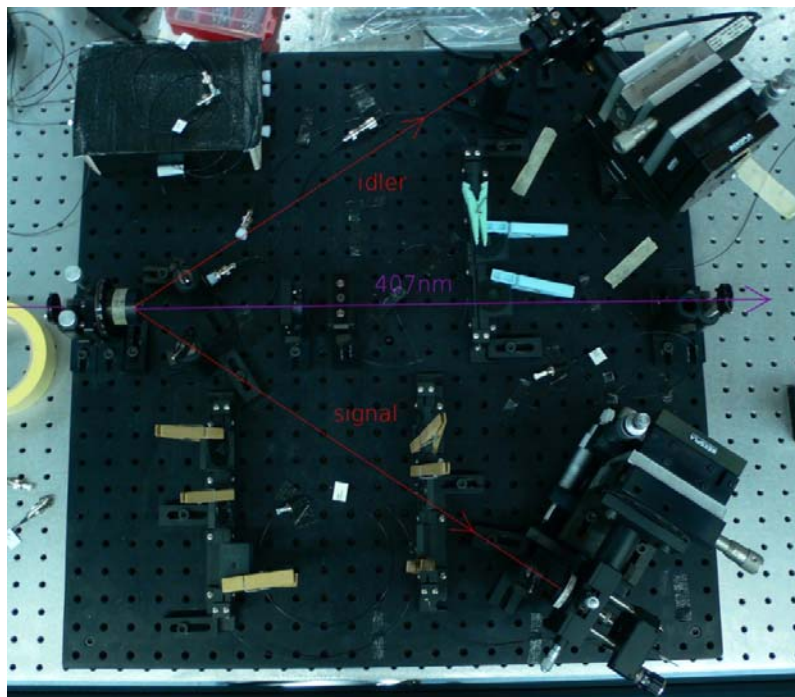
Figure 9: Source. Parametric down-conversion occurs in the lithium iodate crystal pumped by 407nm laser beam (on the left); idler and signal photons are selected and coupled into fibers.

The typical rate of coupled light detection was around 25 000 photons per second. With detector efficiency (as there is always considerable inefficiency) around 60% the real conversion rate in selected directions could be estimated to be around 40 000 photons per second. As photons travel at around $2*10^8$ m/s in fiber, the low photon generation rate ensures a long interval between distinct photons events (5 km or 25 μs) and it is thereupon highly improbable that two photons would enter the

interferometer at a time, in which case both would, being bosons, take the same path. Virtually all signal photons enter the interferometer alone and interfere with themselves.

4.1.2 Interferometer Components

The body of a fiber Mach-Zehnder interferometer consists of two fiber couplers; the first one divides incoming light into two separate fibers, the second one recombines them and divides interfering light into two separate fibers again. Yet in order to optimize interference in the interferometer, it has to be possible to control and manipulate the relative phase difference and polarization of light going through the interferometer arms; that is why other fiber optical components have to be placed inside the arms. We had fiber polarizations controllers, polarizers, phase modulators and an air gap placed in the fiber paths of our interferometer. Relative placement of these components described below can be seen on Figure 8 above.
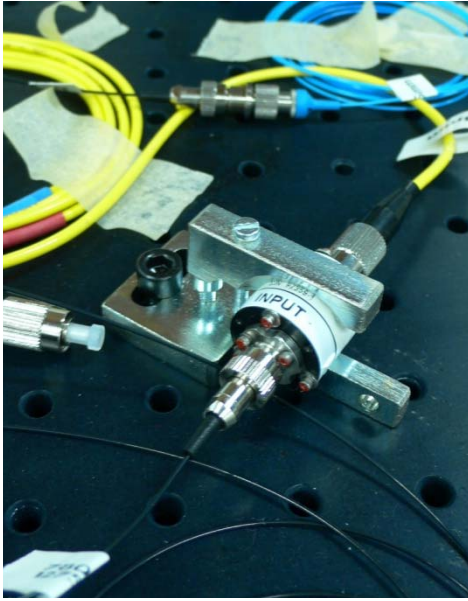
4.1.2.1 Polarizers

Polarizers are devices that change the general polarization state of passing light into a definite polarization state by blocking all components of the electric field vector which are perpendicular to their transmission axis, and letting through only those which are parallel [14]. The polarization of light travelling in a fiber is constantly being altered by birefringence inside the fiber core due to mechanical stress of various origins. The light wave in a birefringent medium splits into two orthogonally polarized waves which see different indexes of refraction; their relative phase therefore changes while they propagate, along with the global polarization state of their superposition [16]. To secure definite polarization in fibers where it is needed polarizers must be utilized and fibers must be fastened (fiber movement and bending changes the stress, birefringence conditions and consequently polarization).

In our setup, we used two polarizers with set (nonadjustable) transmission axes. One (S# 97359-1) was placed before the first fiber coupler to fix the polarization state of light entering the interferometer. Having a stable incoming polarization was very convenient since the adjustment of polarization inside the interferometer arms did not have to be redone every time the polarization outside the interferometer changed, which could happen quite often and easily anywhere in the unprotected fiber linking the source to the interferometer. The interferometer itself was covered by a

polystyrene box, mainly for isolation from thermal fluctuations and air circulation, but also for more stable fiber positions that were crucial for polarization maintenance.

The second polarizer (S# 97359-2) was placed after the phase modulator which did not have an integrated polarizer (labeled PM on Fig. 8), thus replicating the phase modulator with an integrated polarizer in the lower interferometer arm (labeled PMP on Fig. 8). This was again done for adjustment convenience and to ease polarization overlap in the second fiber coupler.

Figure 10: Fiber polarizer.

Several available polarizers were tested for transmission losses before the least costly were selected. Their attenuation was:

Polarizer	Attenuation* [dB]	Transmission
S# 97359-1	0.7369 ± 0.0128	$84.39\% \pm 0.93\%$
S# 97359-2	0.3084 ± 0.0072	$93.15\% \pm 0.84\%$

*Attenuation$= 10 \times log_{10}(\frac{input\ intensity}{output\ intensity})$ [dB]

4.1.2.2 Polarization Controllers

Fiber polarization controllers or the so called "bat ears" are adjustable polarizers which avail of the fiber stress-induced birefringence mentioned above. By coiling fiber, waveplates with specific retardation effects can be created. The retardation between orthogonal polarization components is directly proportional to the coiled fiber length and inversely proportional to the coiling radius [16]. Normally ready-made fiber holders are used that allow to coil the fiber and fasten the coils into movable "ears" (see Figure 11) at a specific radius at which a specific number of turns creates a quarter- or a half-wave plate. These fiber retardation plates are typically placed in a $\frac{\lambda}{4}, \frac{\lambda}{2}, \frac{\lambda}{4}$ sequence, so that when the coils are rotated along the fiber holder

axis, any polarization state can be reproduced. A big advantage of these polarizers is the absence of other losses than those caused by propagation in fibers.
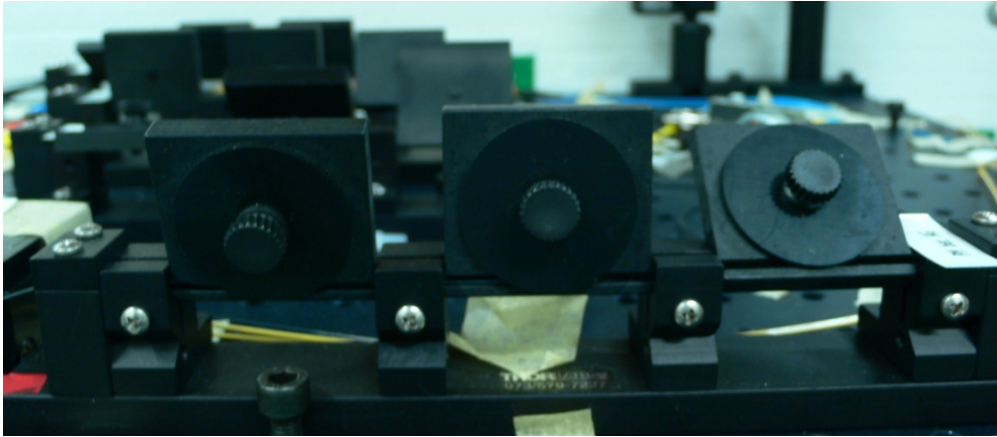

Figure 11: Fiber polarization controllers, also known as "bat" ears.

As shown on Fig. 8, there were four polarization controllers present in our setup. The purpose of three of them (labeled PC, PC 1 and PC 2) was to optimize transmission through the polarizer (PC) and phase modulators (PC 1 and PC 2). Every time the polarization would change in between the source and the interferometer, attenuation through the fixed-transmission-axis polarizer was easy to minimize by adjustment of PC. In what concerns the phase modulators, it is probable that they block almost all of the incoming polarization component perpendicular to its axis. Transmission losses are therefore very large if the polarization state before the modulator is not properly adjusted.

The fourth polarization controller in our setup (PC - P) was a tool for improving polarization overlap in the second fiber coupler where interference occurred. The polarization of light going through the upper interferometer arm would be adjusted with PC – P to match the polarization state in the lower interferometer arm.

4.1.2.3 Adjustable Air Gap

The pre-calculation of paths and selection of right fiber lengths when building the interferometer does not ensure a perfect compensation for paths lengths difference between the two interferometer arms, which is needed to achieve a high visibility. In our case, the coherence length was, according to our estimation, around 15 μm. It was therefore impossible to achieve precise phase matching without sensitive path length manipulation. To enable this, an air gap with adjustable width was placed inside the

upper arm of the interferometer. One side of the gap was mounted on a motorized stage controllable by PC, so the gap scanning for visibility maxima could be done electronically.

The air gap attenuation was measured to be 0.4636 ± 0.0092 dB which corresponds to $90\% \pm 0.87\%$ transmission.

4.1.2.4 Phase Modulators

Electro-optical phase modulators were key to all stages of this project. They allowed fast phase change for all visibility calculations, stabilization procedures and feed-forward implementation. Phase modulation via applied voltage is based on the linear Pockels effect: the refractive index of the nonlinear crystal material inside modulators grows with increasing intensity of applied electric field which delays the light passing through.

As Fig. 8 shows, two modulators were used in our setup, each in one of the interferometer arms. Both the modulator without integrated polarization output control (PM-OK1-00-PFU-PFU-830-S, S# 75815) and the one with an integrated polarizer (PM-OK5-00-PFU-PFUP-830-S, S# 73931) were manufactured by EOSPACE and used lithium niobate for the Pockels effect (see Fig. 12). Both of them were also provided with input and output polarization-maintaining fibers.

For active stabilization of the interferometer and feed-forward implementation precise phase change was needed. Hence half-wave voltages, i.e. voltages which would induce a phase change of π on application, had to be measured for both modulators (for measurement details see Section 5.2). Results can be found in the table below, along with measured attenuation.

Modulator	Attenuation* [dB]	Transmission	Half-wave Voltage
PM	1.7927 ± 0.0241	$66.18\% \pm 1.00\%$	1.435 ± 0.005 V
PMP	4.5442 ± 0.0461	$34.64\% \pm 0.90\%$	1.535 ± 0.005 V

*Attenuation$= 10 \times log_{10}(\frac{input\ intensity}{output\ intensity})$ [dB]

Phase modulators were controlled electronically from the PC through multiple channel Advantech analog output card (PCI-1723) which was operated using MATLAB. Throughout the first part of the project PM was used for all interferometer

optimization and stabilization procedures. When feed-forward was tested, PMP was used for stabilization and PM for feed-forward control.
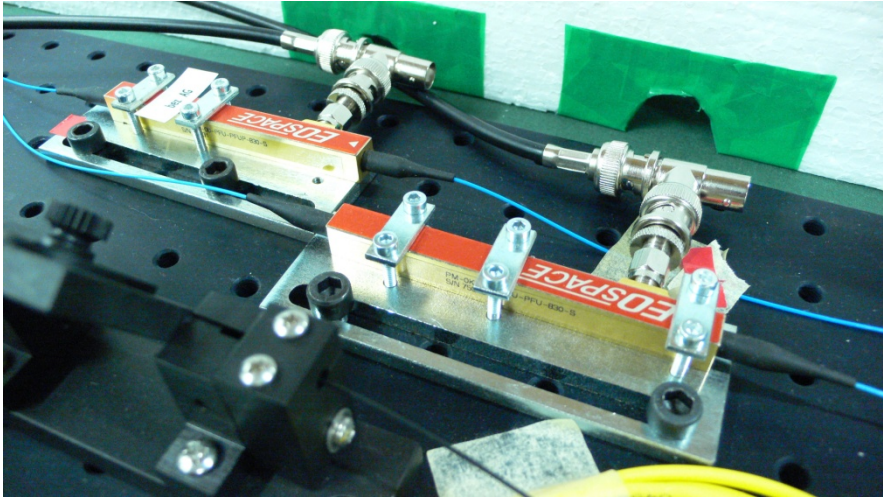

Figure 12: Lithium niobate phase modulators from EOSPACE.

4.1.2.5 Fiber Couplers

Fiber couplers are devices provided with input fibers and output fibers which combine and divide incoming optical power by twisting, tapering, fusing or melting the fibers, according to a fixed or a variable ratio. The power distribution ratio in general depends on wavelength and polarization of light.
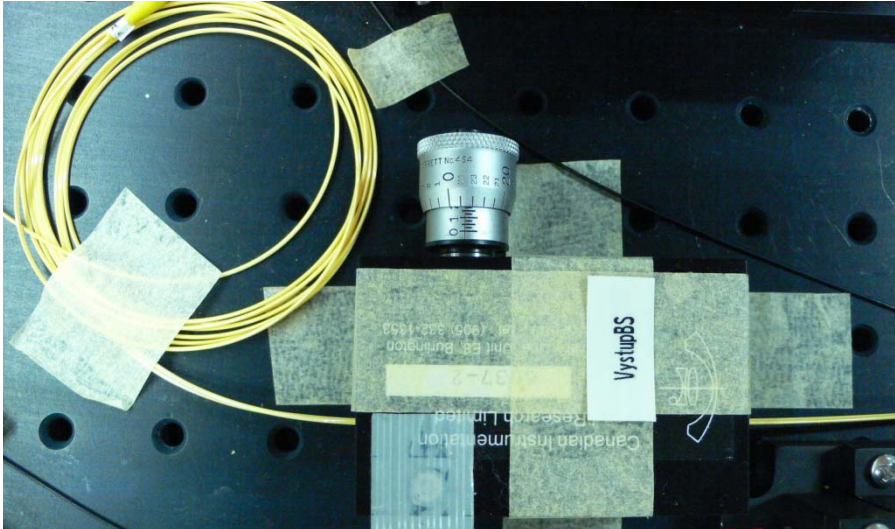

Figure 13a: Variable ratio coupler from Canadian Instrumentation and Research.

The fiber coupler leading photons into our Mach-Zehnder interferometer had a fixed 50:50 coupling ratio, so that the optical power coming through one of its inputs would be divided equally between the outputs while the other input was left unused

(see setup on Fig. 8). Interference occurred in the variable ratio coupler (VRC) which was equipped with a screw gauge whose rotation would change the coupling ratio. A method for determining the coupling ratio of the output fiber coupler is described in Section 5.1.
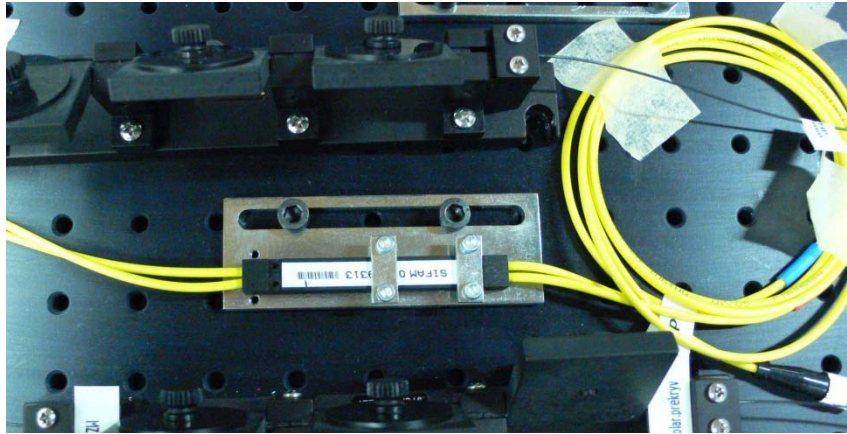

Figure 13b: Fixed ratio 50:50 fiber coupler from Sifam Fibre Optics.

The two fiber couplers we used in our setup were from Sifam Fibre Optics (fixed 50:50 ratio coupler at the interferometer input, see Fig. 13b above) and Canadian Instrumentation and Research, Ltd. (the variable ratio coupler at the interferometer output, see Fig. 13a above).

4.1.3 Detectors

Experiments operating at a single-photon level need detectors that allow for detection of single photons. A straightforward means of detection is to avail of the photoelectric effect and count the electron-hole pairs generated by incident photons. Naturally the current produced by a single photon is microscopic and has to be amplified in order for the detector to produce a measurable voltage pulse every time an event occurs. This amplification can be done in different ways.

The detectors we used in our experiment were APDs (Avalanche Photodiodes) operating in the Geiger mode: a four-detector counting module array SPCM-AQ4C and a single detector SPCM AQR-14FC 13610 from Perkin Elmer Optoelectronics (See Fig. 14a and b). In this type of single-photon detectors generated photoelectrons/holes are accelerated with barrier voltage, ionize the medium and produce more photoelectrons/holes when they gain enough energy. The avalanche process has to be quenched at the right time by electronics or controlled by a load resistance which sets a maximum current otherwise a breakdown will occur and

destroy the diode. The output of the detectors we used was in the form of positive logic 4.5V TTL pulses (transistor-transistor-logic standard).

There are several important detector parameters which have to be considered when data are acquired and worked with: dead time, detector efficiency, dark counts, and duration of detector response. Dead time defined the amount of time needed between two detection events so that they can be distinguished (the time interval after each event during which the detector is unable to respond). The detectors we were working with it is usually have a dead time of the order of tens of nanoseconds [15]. In practice dead time can be regarded as a type of detector inefficiency. As the separation between photon events in our case was of the order of tens of microseconds (as discussed in Section 4.1.1), dead time was not an issue.

Detector efficiency depends on the probability of electron-hole pair formation, probability of material ionization by accelerated electrons or holes and losses from reflection inside the detection medium. Typical efficiency for the type of detectors we used should be around 50% for 814nm we were operating at (see Appendix or CD enclosed to this paper for SPCM-AQ4C data sheet). The two detectors we used, apart from the auxiliary APD detector utilized for feedback in the feed-forward setup, were part of a four-detector APD module. Only relative efficiencies were of interest for us so that we could compare the data obtained at the two interferometer output. The relative efficiencies were measured with respect to detector 2:

Detector	Relative efficiency
0	0.9908
1	0.7343
2	1.0000
3	0.9999

The detector noise, usually referred to as dark counts, is also an important issue when signals at different outputs are compared, because every detector has a particular amount of noise, and when we need to know the actual value of interferometric visibility (recalling the visibility definition (6), if dark counts are not subtracted, the measured V value would be lowered by the amount of 1/(2*amount of

dark counts per appropriate unit time))[4]. During interference optimization, we subtracted appropriate amounts dark counts in all our measurement procedures. As dark counts fluctuate with temperature, they had to be re-measured before every set of measurements (the amount of dark counts could be expected to stay stable for several hours). Average values of dark counts per second[5] were around 400 ± 10 for detector 2, 320 ± 10 for detector 3 and 160 ± 1 for the auxiliary detector used in the setup for feed-forward testing (see Fig. in Section 4.2).

The duration of detector response had to be known for feed-forward control timing (see Section 4.2). We readily used the results available from [17]; response of the SPCM AQR single detectors was measured to be 17 ns long.
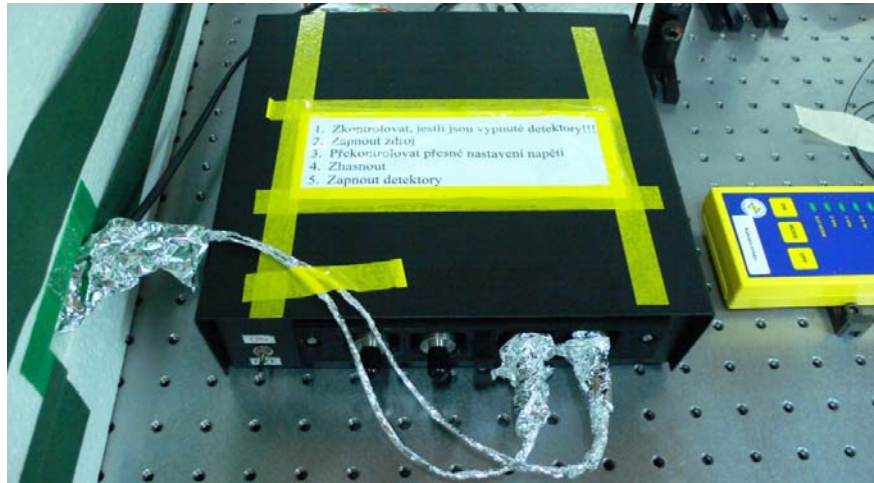
Figures 14a and b: APD detectors SPCM-AQ4C (above) and SPCM AQR-14FC (below).

---
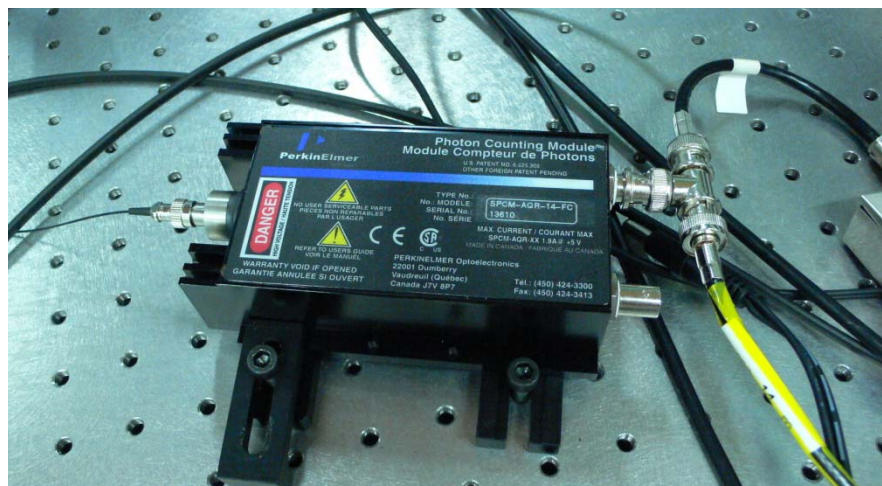
[4] The calculated value of visibility could also be lowered by noise coming from out of the fibers (yellow fiber jackets unlike the black ones do not completely isolate the fiber core); that is why output fibers were covered with aluminium foil, as seen on Fig. 12a.

[5] When measuring dark counts, we would always average over 100 values of # of dark counts per second to compensate for fluctuations due to the presence of certain randomness in the detection process.

It is logical that single photon detectors such that have been described above have to be very sensitive to light. For this reason and in order to minimize noise, all measurements were made in the dark.

4.1.4 Counter

Data from detectors in the form of positive voltage TTL pulses per unit time were acquired, counted and communicated to the PC by a counter. The counter was an Ortec 974 100 MHz Quad Counter/Timer (see Fig. 15) with four input channels, one of which was employed as a timer to preset counting time. TTL pulses from the detector had to be converted to the NIM (Nuclear Instrumentation Module) logic standard, which has the form of short negative pulses, before entering counter inputs that were NIM standard based.

The counter was controlled and read from through a serial port using the MATLAB computing environment (version 7.10). All our measurement procedures were thus programmed in MATLAB (see CD in Appendix for codes).
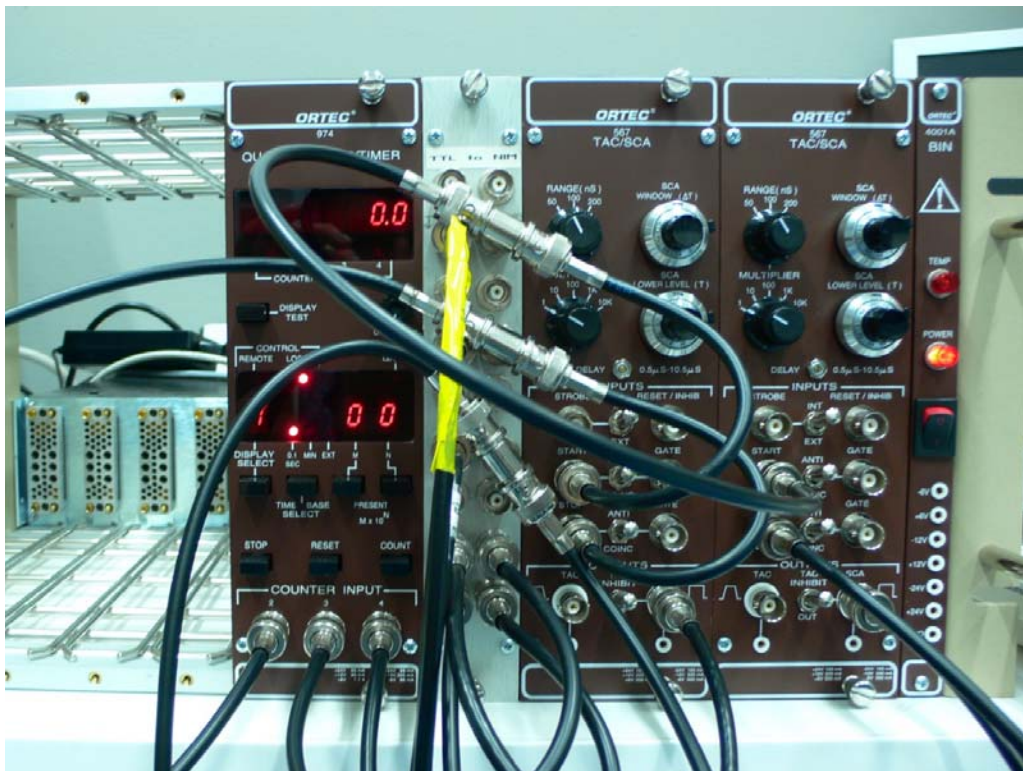

Figure 15: ORTEC Quad Counter/Timer 974 (on the left). TTL to NIM converter in the middle and ORTEC TAC/SCA (time-to-amplitude converter and single channel analyzer) 567 for coincidence measurement on the right.

4.2 Setup for Feed-Forward Testing

The purpose of feed-forward is to induce a phase shift of π between the available states of the qubit, as explained in Section 1.3. When translated to the experimental reality of the Mach-Zehnder qubit implementation, where the situation of perfect phase matching ($\delta = 0$) between interferometer arms corresponds to constructive interference at one of the detectors and destructive interference at the other, inducing a phase shift of π (now $\delta = \pi$) between 0 and 1 states of the qubit effectively means switching between maxima and minima at the interferometer outputs. The feed-forward control in fact operates as a switch: when it is present, the detector that normally reads a minimum shows a maximum and vice versa.

However, we must not forget that this holds only in the case of an ideal optimized and stable interferometer. In the real case the minimum at one of the outputs will never be exactly zero but with visibilities around 96% we are only able to bring it close enough to zero. This is why high visibilities were needed for our feed-forward demonstration.

The setup for feed-forward testing (see Figure 16) avails of the idler photon generated by the source along with the signal one: when it is detected by the auxiliary detector AD, feedback from the detector in the form of a voltage pulse is scaled to the half-wave voltage value and applied via the phase modulator PM.

Yet the scheme on Figure 16 does not include the fact that not just intensities (numbers of counts) but coincident detections were measured. We wanted the phase shift to be applied to the signal photon if and only if its counterpart with which it was entangled was present in the control line. It was also probable that some of the idler photons might have got lost on their way, their signal twin reaching interferometer outputs meanwhile, which would result in unreadable switching of maxima and minima at the detectors. To discard all uncorrelated detection cases coincidence measurements were used. This means that the counter would count only those events when the recorded time interval between detections at the auxiliary detector and detectors 2 and 3 was within a predefined narrow window. Coincidence detection is described in more detail in Section 6.3.
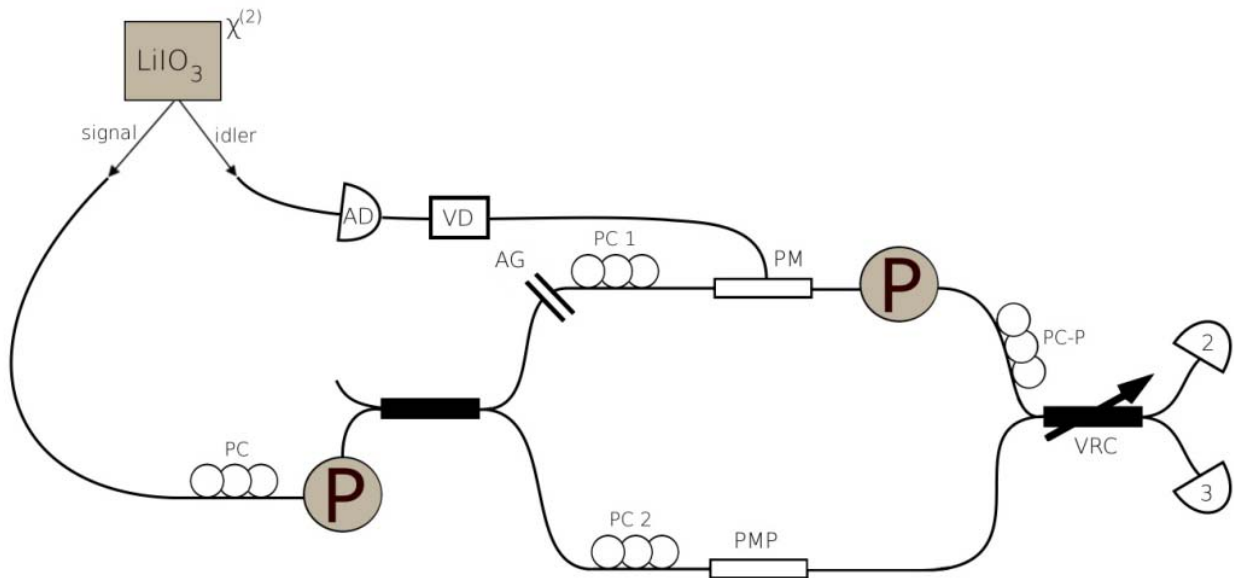
Figure 16: setup for feed-forward testing. AD – auxiliary detector, VD – voltage divider. The idler counterpart of the signal photon gets detected by detector AD and the scaled pulse is lead to a phase modulator in the upper interferometer arm.

4.3 Final Setup Outline

A simplified scheme of the programmable phase gate based on encoding of qubits into spatial modes and Mach-Zehnder interferometers, that we are planning to build with the application of feed-forward control, can be found here below (Fig. 17):
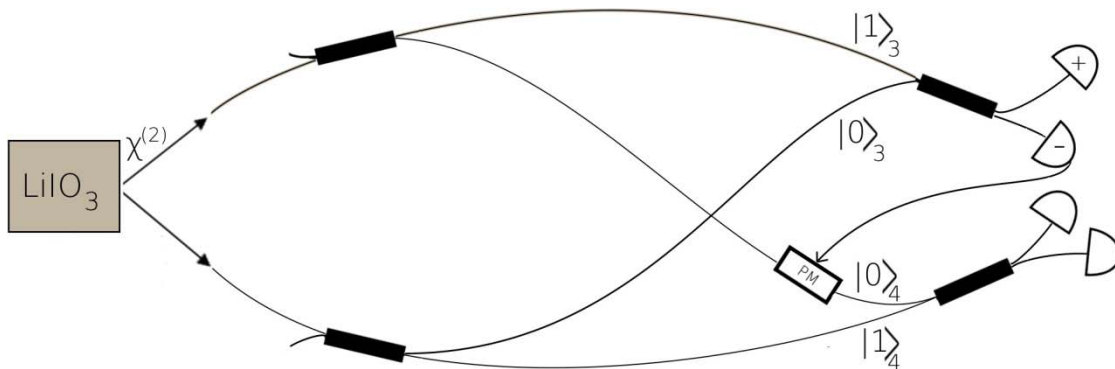
Figure 17: a simplified scheme of the programmable phase gate setup built with fiber optics. Beamsplitter transmitting states 0 and reflecting states 1 is constructed by means of two intertwined Mach-Zehnder interferometers. PM – phase modulator.

As was explained earlier in this text, the core of the programmable phase gate is a theoretical beamsplitter that transmits one of the basis states and reflects the other (see Section 1.3). A similar beamsplitter can be effectuated in different ways. The

approach that we take is based on two intertwined Mach-Zehnder interferometers. The program and data qubits $|\psi\rangle_{PRG} = \frac{1}{\sqrt{2}}\left(|0\rangle + e^{i\phi}|1\rangle\right)$ and $|\psi_{IN}\rangle_{DAT} = \alpha|0\rangle + \beta|1\rangle$ are prepared by the first two fiber couplers (after the source on the left at Fig. 17). The other two fiber couplers (on the right side of Fig. 17) set the measurement bases. The signal and idler photons coming from the source both enter different interferometers, but pairs of modes corresponding to states $|1\rangle_1$, $|0\rangle_2$ and $|1\rangle_2$, $|0\rangle_1$, where indices 1 and 2 indicate the upper and the lower interferometer respectively, are cross-coupled by another two fiber couplers. This can be understood as an equivalent of the situation where two superpositions of states 1 and 0 meet at a beamsplitter which transmits states 0 and reflects states 1, so two combinations of states 0 and 1 originating from different qubits emerge at the two outputs of the beamsplitter. In this way our setup follows the principle described in Section 1.3 of this paper.

If detector labeled (-) clicks, a phase shift of π is applied by feed-forward control via a phase modulator to the quantum state that exists before the lower fiber coupler.

5 Experimental Methods for Interferometer Adjustment

In the first place, three basic steps had to be taken to meet all necessary conditions for the operation of feed-forward control: interference contrast had to be optimized and interferometer outputs balanced, the values of half-wave voltage for both phase modulators in our setup had to be determined and a working active stabilization procedure elaborated.

5.1 Interference Optimization

It has already been explained in the previous section why high interference contrast was needed in order for the feed-forward control to operate. The visibility of a Mach-Zehnder interferometer is optimal if the optical path lengths in both interferometer arms and the intensities[6] of interfering waves are equal, and if polarization overlap is achieved at the output beamsplitter. In our setup, the tool for altering the path lengths difference was an adjustable air gap; appropriate air gap width thus had to be found. The balance of interfering light intensities was accomplished by compensating transmission losses of interferometer arms and polarization overlap was reached by adjusting polarization controllers before the output fiber coupler (PC – P on Fig. 8). However, because fibers are extremely sensitive to bending and twisting, every disconnection and reconnection of a fiber usually alter the polarization and moreover, rejoining of a fiber and a connector may slightly change transmission through the connection point, it is advisable to follow the successive steps of the optimization procedure in a specific order if they are not to be repeated in vain.

5.1.1 Optimizing Transmission through the Interferometer

To maximize the precision of interferometric measurement and later of the feed-forward operation, transmission through the device had to be optimal. The Poisson uncertainty in the number of counts C is $\delta C = \sqrt{C}$, so for a small number of counts the uncertainty is comparable to the number itself and he information that the number gives us loses its value.

Appropriate adjustment of the first set of polarization controllers (labeled PC on Fig. 8) selecting a polarization state in line with the polarizer transmission axis would

---

[6] When speaking of intensities, we mean the count rate obtained.

maximize transmission through the polarizer before the first fiber coupler. While the controllers were being adjusted, measurements of the numbers of counts per second detected by detectors 2 and 3 were made via programs written in the MATLAB environment, so that the sum of counts per second at detectors A and B could be read in real time in the MATLAB Command Window (see CD in Appendix for codes). Each one of the three bat ears was rotated until the sum of count rates at detectors A and B was at its maximum.

In the next stage, the controllers PC 1 and PC 2 were adjusted until a maximum sum of counts at detectors 2 and 3 was obtained again; this meant that the polarization-sensitive transmission through phase modulators PM and PM − P and thus transmission through the arms of the interferometer were optimized.

The usual maximum number of counts per second transmitted through the interferometer was around 2300 counts. This would reduce to around 2100 during the feed-forward operation as more fiber had to be added in the signal photon path and each additional fiber connector would bring about more transmission losses.

5.1.2 Setting the Output Coupling Ratio on 50:50

In the beginning of the optimization procedure, the interferometer outputs had to be balanced by setting the coupling ratio of the output coupler to 50:50. Without a balanced intensity distribution we would not be able to reach desired visibilities (above 90%) at both of the output detectors.

If we block transmission through one of the interferometer arms, the ratio of intensities (numbers of counts) at the output detectors will not be equal to the coupling ratio because the detection efficiencies are in general different. To take efficiencies into account, we used the following method (see Fig. 18): let X and Y be the input paths corresponding to interferometer arms, FC the fiber coupler, 1 and 2 the output paths corresponding to interferometer outputs with detectors, ξ_X, ξ_Y the efficiencies of transmission through the input paths and ξ_1, ξ_2 the efficiencies of transmission through the output paths corresponding to the efficiencies of detectors.

Let R and T be the intensity reflection and transmission coefficients respectively. Energy has to be conserved so R fully determines T and vice versa:

$$R + T = 1 \, .$$

The intensity I_X of the light wave coming along path X gets split by the fiber coupler into a reflected part and a transmitted part

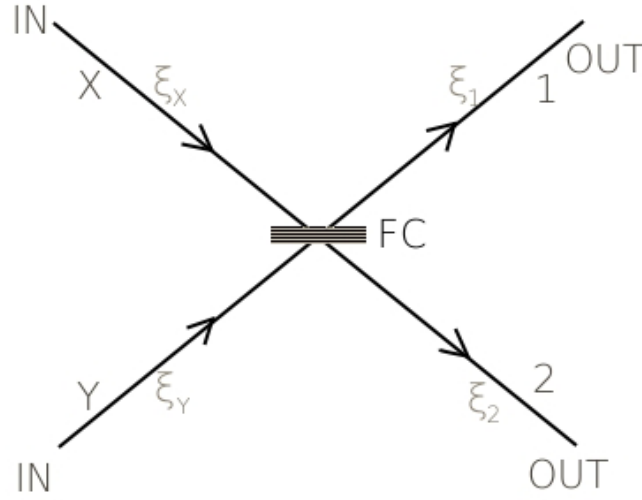$$I_{X1} = \xi_X \cdot R \cdot \xi_1 \cdot I_X$$

Figure 18: Illustration for the method of determining the coupling ratio of fiber coupler FC. All the efficiencies ξ have to be taken into account.

$$I_{X2} = \xi_X \cdot T \cdot \xi_2 \cdot I_X,$$

the intensity I_Y of the light wave coming along path Y gets split into

$$I_{Y1} = \xi_Y \cdot T \cdot \xi_1 \cdot I_Y$$

$$I_{Y2} = \xi_Y \cdot R \cdot \xi_2 \cdot I_Y \, .$$

If we calculate the number $\alpha = \frac{I_{X1} \cdot I_{Y2}}{I_{X2} \cdot I_{Y1}}$, the intensities I_X and I_Y and the efficiencies cancel. We get

$$\alpha = \frac{I_{X1} \cdot I_{Y2}}{I_{X2} \cdot I_{Y1}} = \frac{\xi_X \cdot R \cdot \xi_1 \cdot I_X \cdot \xi_Y \cdot R \cdot \xi_2 \cdot I_Y}{\xi_X \cdot T \cdot \xi_2 \cdot I_X \cdot \xi_Y \cdot T \cdot \xi_1 \cdot I_Y} = \left(\frac{R}{T}\right)^2 = \frac{(1-T)^2}{T^2}.$$

Hence T can be calculated knowing α by solving the quadratic equation:

$$(1-\alpha)T^2 - 2T + 1 = 0,$$

which has two solutions

$$T_{1,2} = \frac{1 \pm \sqrt{\alpha}}{1-\alpha} = \frac{1 \pm \sqrt{\alpha}}{(1-\sqrt{\alpha})(1+\sqrt{\alpha})}$$

out of only one always gives a meaningful physical result for T (>0 and <1), depending on whether R is < or > than T.

We were able to calculate α easily by measuring the intensities I_{X1}, I_{X2}, I_{Y1}, I_{Y2}. I_{X1} and I_{X2} could be read at detectors 2 and 3 corresponding to paths 1 and 2 if transmission through the interferometer arm corresponding to Y was blocked; intensities I_{Y1} and I_{Y2} were obtained if the arm corresponding to X was obstructed.

The coupling ratio of the VRC was adjusted by means of a screw gauge and intensities were measured with the upper and lower interferometer arms blocked in terns until $T\epsilon \langle 0.5 - \delta T, 0.5 + \delta T\rangle$, where $\delta T = \sqrt{(\frac{\partial T}{\partial \alpha} \cdot \delta\alpha)^2} = \frac{\partial T}{\partial \alpha} \cdot \delta\alpha$, which was around 1-2 %. Adjustment of the screw mechanism was lengthy because it exhibited considerable hysteresis.

Measurement of the coupling ratio would be inconvenient at a later time, because while the upper interferometer arm could be cut off by simply blocking the air gap with non-transparent material, the lower arm required disconnecting fibers which would, as mentioned above, usually change the polarization and thus deteriorate transmission through the interferometer, in which case transmission optimization would have to be performed again.

5.1.3 Compensating Transmission Losses between Interferometer Arms

Balancing intensities going through the arms of the interferometer in principle means to bring about additional transmission losses in the more efficient arm. To determine the losses needed we would measure the average sum of count rates at detectors 2 and 3 with and without the upper interferometer arm blocked which correspond to the intensity going through the lower arm and the intensity going through both arms respectively. If the intensity through the lower arm is subtracted from the intensity through both arms, intensity through the upper arm is obtained. We would then induce losses in the arm which transmits higher intensities by adjusting the polarization with polarization controllers before one of the phase modulators, so that the intensities were equal.

If I_U is the intensity that is transmitted or lost in the upper interferometer arm and I_L the intensity transmitted or lost in the lower arm, the intensities that meet at the output fiber coupler are $I_U \cdot \xi_U$ and $I_L \cdot \xi_L$ where ξ are the corresponding

35

efficiencies of transmission. ξ_2 and ξ_3 are the detection efficiencies of detector 2 and 3. If the sum of count rates at both detectors is measured when none of the arms is blocked, the result would correspond to

$$\xi_2 \cdot \xi_3 (I_U \cdot \xi_U + I_L \cdot \xi_L).$$

If it is measured with the upper arm blocked, the result corresponds to

$$\xi_2 \cdot \xi_3 \cdot I_L \cdot \xi_L.$$

If we subtract this from the previous result we get

$$\xi_2 \cdot \xi_3 (I_U \cdot \xi_U + I_L \cdot \xi_L) - \xi_2 \cdot \xi_3 \cdot I_L \cdot \xi_L = \xi_2 \cdot \xi_3 \cdot I_U \cdot \xi_U.$$

We need $I_U \cdot \xi_U$ to be equal to $I_L \cdot \xi_L$, naturally this would occur when $\xi_2 \cdot \xi_3 \cdot I_U \cdot \xi_U = \xi_2 \cdot \xi_3 \cdot I_L \cdot \xi_L$.

We thus induced losses in the arm with higher $I \cdot \xi$ and repeated the measurement until the desired equivalence was obtained.

5.1.4 Compensating for Arm Lengths Difference

The air gap in the upper arm of our Mach-Zehnder interferometer had one of its sides placed on a motorized stage; it was therefore possible to change the length of the upper arm by changing the width of the air gap and in this way compensate for arm lengths differences. To find the right width allowing the best interference contrast, the air gap had to be scanned while visibilities were measured for both detectors at each of the motor positions.

5.1.4.1 Visibility Measurement

Visibility can be calculated from a maximum and a minimum of a fringe (see (1)). In our case the fringes constituted of a series of data in the form of count rates which were measured for a set of phase differences between the interferometer arms. The phase could be varied by applying voltage via an analog output card on one of the phase modulators in one of the arms of the interferometer. A certain value of voltage would induce a phase shift of π – this value is called the half-wave voltage, U_π, and it is in general different for different modulators[7]. If a sequence of voltage values is applied on a phase modulator in the range - U_π and + U_π while intensity is recorded at

---

[7] For the modulators in our setup, this was around 1.4V (for precise data see Section 4.1.2.4).

both of the interferometer outputs, it should be theoretically possible to reconstruct a fringe with a maximum and a minimum from the acquired data. In reality, a phase drift is always present and scanning the interval from $-U_\pi$ to $+U_\pi$ for intensities might not produce enough data with visible extremes. That is why we did not need the exact value of U_π and usually applied voltage values in a wider range[8] with between 70 and 100 steps, so that we would get between 70 to 100 count rates for each of the detectors. If we plotted count rates against applied voltage values, we would get similar fringes as those shown on Figure 19 here below.
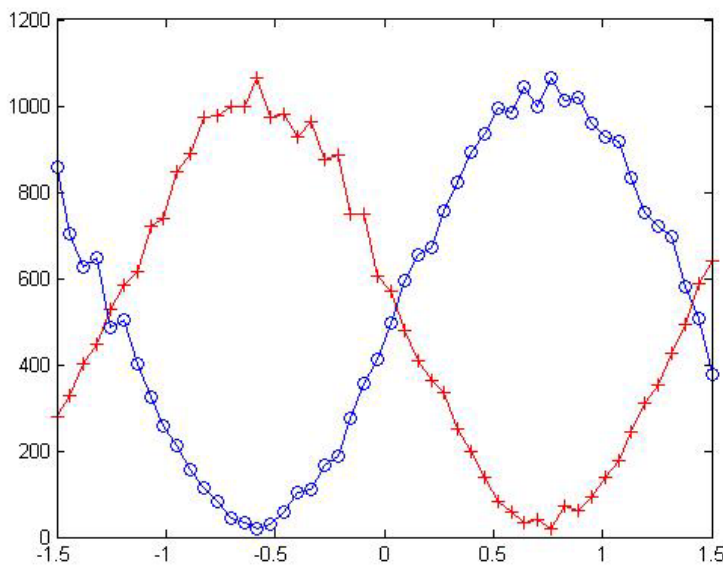

Figure 19: Interference fringes. Number of counts per second vs. applied voltage.

5.1.4.2 Air Gap Scanning

The motor which could move one of the coupling lens holders was controlled through a serial port using MATLAB. The program for air gap scanning would make the motor move in a range and with a step defined as program inputs and measure the visibilities. The visibilities for different motor positions would be recorded and the motor would be placed at the position where a maximum visibility was obtained. A sketch[9] of the procedure would be:

```
GAP_SCAN(range, step)
open counter, set counter
open motor
open analog output card
for i=range(min):step:range(max)
```

```
data=empty matrix;
visibilities=empty matrix;
     for j=voltage(min):( voltage/70): voltage(max)
     send voltage(j) to modulator
     intensity=count for 1s
     append [j intensity] to the matrix data
     end
     calculate m=maximum of data
     calculate n=minimum of data
     append [i (m-n)/(m+n)] to the matrix visibilities
     end j
end i
find p=motor position for max(visibilities)
move motor to p
```

See CD in Appendix for codes of QUAD_MERENI_POSUV_BEZFITOVY.m .

As the coherent length for our source was, according to our estimation, around 15 μm, scanning the air gap by steps of less than 1 μm around the position of maximum interference contrast would produce similar results and was thus usually useless.

5.1.5 Adjusting Polarization Overlap

After losses are compensated and arm lengths balanced, the visibility can only be improved by polarization overlap improvement. To adjust polarization state of light going through the upper interferometer arm, so that it would overlap with the polarization state of light going through the lower arm, bat ears before the output fiber coupler (PC – P on Figure 8) were rotated. To see whether interference contrast improved visibility had to be measured every time an adjustment of one of the polarization controllers was performed, which made the process quite lengthy in comparison to a high-signal case where visibility can be estimated right away using an oscilloscope.

5.2 Half-wave Voltage Measurement

It is not necessary to know the exact value of half-wave voltage during interference optimization as long as fringes minima and maxima can be read, but the information is crucial for stabilization when precise phase shifts have to be applied.

The method for determining half-wave voltage is based on the fact that when a phase shift of 2π is applied in one of the interferometer arms, the intensity observed at the outputs should not be altered (the situation is equivalent to moving from one position on a fringe to the same position on a neighboring fringe). Consequently, the intensity measured when U_π is applied should be equal to the intensity measured when $-U_\pi$ is applied. It should be therefore possible to evaluate half-wave voltage by comparing intensities for negative and positive voltage values applied on the phase modulator, taking small enough steps within a big enough range.

However, random phase fluctuations and error of measurement make the determination of half-wave voltage more difficult. To minimize the effect of phase drift, it was more convenient to make several shorter counts for voltages alternating between U_π and $-U_\pi$, add them up to obtain the usual count rates per second and then calculate the absolute value of their difference. To minimize the effect of measurement error, we averaged over a large number of measurements (between 500 to 1000). A simplified scheme[10] of the MATLAB program we used for half-wave voltage evaluation would thus be:

```
HALF_WAVE_VOLTAGE(voltage, step)
Note: voltage=range of voltage values to be scanned
open counter, set counter
open analog output card
for i=voltage(min):step:voltage(max)
  for j=1:number of measurements
  intensity_plus=0;
  intensity_minus=0;
      for k=1:10
      send voltage(i) to modulator
      intensity=count for 0.1s
```

---

[10] This is again a very simplified illustration of the procedure logic.

```
            intensity_plus=intensity_plus+intensity

            send -voltage(i) to modulator

            intensity=count for 0.1s

            intensity_minus=intensity_minus+intensity

        end k

    difference=absolute value(intensity_plus - intensity_minus)

    data(i,j)=difference

    end j

    mean(i)=mean of data(i) over all j

end i

plot mean(i) vs. i
```

The need for a larger statistical ensemble of data caused the evaluation of half-wave voltage to be very lengthy – measurements for 5 voltage values would take more than 12 hours. Moreover, the serial port communication between the computer and the counter tended to collapse during long operation; this problem was eventually solved by adding a command which restarted the serial port after every set of twenty measurements for one voltage value. See CD in Appendix for program code (QUAD_PULVLNKA_1.m).

Half-wave voltage values for modulators PM and PMP (as labeled on Fig. 8) were found to be 1.535 and 1.435 $\pm$ 0.005 V respectively (see Appendix for figures).

When working with mean values (we would average over n=at least 500 absolute values of intensities differences), to decide on the results, we also had to evaluate the error of mean estimation which was taken for

$$\sigma = t_\alpha \frac{std}{\sqrt{n}}$$

where *std* stands for standard deviation from the mean ($std = \sqrt{\frac{1}{n-1}\sum_{j=1}^{n}(x_j - \bar{x})^2}$, $\bar{x}$ being the estimated mean value and x_j the result of the j-th measurement), n is the number of measurements and t_α is the critical t-value of Student's t-distribution. The real mean value lies within $\langle \bar{x} - \sigma, \bar{x} + \sigma \rangle$ with probability 1$-\alpha$. We took $\alpha = 0.001$, for which $t_{0.001} = 3.3$. Figures A2 a and b in the Appendix show results together with corresponding error bars centered on the estimated mean values and 2* σ long [18].

5.3 Active Interferometer Stabilization

The drift of phase caused by fluctuations of temperature, air circulation and other mechanical effects cannot be completely ruled out by simply isolating the interferometer in a polystyrene box. It is clearly impossible to implement a logical gate or a switch with an unstable interferometer if no active correction of phase is performed. Thereupon, a functional stabilization procedure which would automatically check and correct the phase after a short enough amount of time and in this way maintain maxima or minima at the outputs of detectors was essential for our project.

The stabilization procedure works with the visibility value and minima on one of the detectors, so it is carried out on one of the outputs only. Before every measurement that employs active stabilization visibility has to be determined and the value stored for the purposes of the stabilization procedure. A fringe is measured[11], visibility calculated and minimum and maximum intensity values I_{min} and I_{max} together with corresponding voltages saved. The stabilization process starts with setting the phase in one of the interferometer arms using the value of voltage U_{min} that corresponded to a minimum during the last visibility measurement. Intensity I_o is measured and normalized into y_0 according to:

$$y_0 = \frac{I_0 - I_{min}}{I_{max} - I_{min}} = \left(\frac{I_0}{I_{tot}} - \frac{1-V}{2}\right) \cdot \frac{1}{V},$$

where $I_{tot} = I_{max} + I_{min}$ and V is the visibility; so $0 \le y_0 \le 1$. This normalized intensity is compared to a limit value *lim* which defines the maximum allowed deviation from the last minimum in terms of the amplitude $I_{max} - I_{min}$; in our stabilization procedure we had *lim* set to 0.01 = 1%. If y_0 is found to be bigger than *lim*, it means that the phase has drifted by more than $\pi/100$ (0.05% of a full cycle) and thus must be corrected. The amount of drift, that is, the value of deviation from last minimum can be determined from the sinusoidal characteristics of interference fringes, when a phase shift of $\pi/2$ is added to the actual phase induced by the phase modulator (see Figure 20). Once more, intensity is measured and normalized:

---

[11] When stabilizing, we would never subtract dark counts from measured count rates to observe real fringes minima. This would deteriorate the calculated value of visibility, but would not obstruct the procedure.

$$y_{\pi/2} = \frac{I_{\pi/2} - I_{min}}{I_{max} - I_{min}}$$

and the angle $\alpha = \arcsin(2y_{\pi/2} - 1)$ is calculated[12]. There are two cases of phase deviation δ corresponding to y_0 being smaller or bigger than 0.5:

if $y_0 \leq 0.5$, $\delta = \alpha$ (case #1, depicted at Fig. 17)

if $y_0 > 0.5$, $\delta = \pi - \alpha$ (case #2).

We are now able to recalculate U_{min} which would get us back to minimum intensity, according to the specific case:

$$U_{min}' = U_{min} - \frac{\alpha}{\pi} \cdot U_\pi \qquad \text{(case \#1)}$$

$$U_{min}' = U_{min} - \frac{\pi - \alpha}{\pi} \cdot U_\pi \qquad \text{(case \#2).}$$

If the new U_{min}' is applied, y_0 should now be smaller than the limit lim. However, in reality this does not always happen and more stabilization cycles (typically 2-3) have to be run before y_0 satisfies the condition. If $y_0 > lim$, the procedure may go back to the beginning to try again. The starting value of U_{min} will be U_{min}' from the last stabilization cycle.
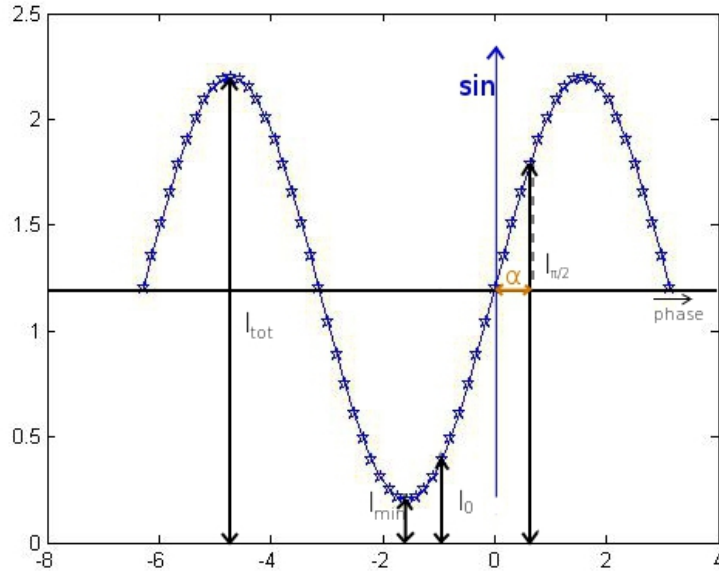

Figure 20: Illustration for calculating the phase deviation. If I_o is bigger than I_{min} by more than 1% of the amplitude I_{max}-I_{min}, phase correction must be applied. The deviation corresponding to phase(I_o) − phase(I_{min}) is calculated by means of $I_{\pi/2}$.

---

[12] Note that the factor of two in the argument of *arcsin* is needed because when normalized, the intensities of our interference fringes run from 0 to 1, whereas the *sine* function runs from -1 to 1.

It may also happen that after performing a number of cycles, the stabilization procedure does not succeed in adjusting the phase to make y_0 close enough to the minimum. The cause of this might be that the visibility V has, for various reasons, deteriorated, so y_0 cannot be properly calculated. If the procedure, after a preset number of cycles, lowers the visibility value by, say, 4 standard deviations, the problem might be solved. Nevertheless, it still might happen that after a new value of V was estimated, the procedure still is not successful. A new proper visibility measurement has to be done and if the visibility is found to be too low, the air gap has to be scanned for new maxima.

A sketch of the program we used to implement the stabilization method described so far would use the following logic (here we suppose that a visibility measurement preceded stabilization and recorded the values of V, I_{min}, I_{tot} and U_{min}):

```
open analog output card
open counter, set counter
send Umin to modulator
intensity=count for 1s
if intensity < Imin-chyba(Imin) ¹³
    Imin=intensity, Itot=Imax+Imin, V=(Imax-Imin)/(Imax+Imin)
end
y0=((intensity/Itot)-((1-V)/2))/V
if lim < y0
    while lim < y0
        if # of stabil. cycles performed < max_cycles allowed
            U=Umin+halfwaveV/2 ¹⁴
            send U to modulator
            intensity in pi/2=count for 1s
            ypi2=((intensity in pi/2/Itot)-((1-V)/2))/V
            alfa=asin(2*ypi2-1)
             if y0 <= 0.5
                 Umin=Umin-(alfa/pi)*halfwaveV;
             else
```

---

[13] A similar correction of I_{max} was made if the *intensity* was found to be bigger than the original I_{max}.
[14] Scaling of U for the case $U \notin \langle -U_\pi, U_\pi \rangle$ present in the program was omitted in this rough scheme.

```
                    Umin=Umin-((pi-alfa)/pi)*halfwaveV;
             end
          send Umin to modulator
          intensity=count for 1s
        y0=((intensity/Itot)-((1-V)/2))/V
      elseif # of stabil. cycles performed = max_cycles allowed
           if visibility has not been lowered yet
              V=V-4*chyba(V)
              add additional cycles to max_cycles allowed
           else
              measure visibility, save as V
              if V < 40%
              scan the air gap
              if V still not good, display error and close
              program
              end
           end
      else (# of stabil. cycles performed > max_cycles allowed)
           The interferometer cannot be stabilized.
           display error and close program
      end
   end (while lim < y0)
end (if y0<lim)
```

See CD in Appendix for precise codes (STABILIZACE.m).

A measurement of interferometer stability was performed: after a successful stabilization, count rate was measured for ten minutes on one of the detectors (see Figure A3 in Appendix). A phase drift of approximately $0.005\,\pi$ per second was observed. We concluded that measurements between phase corrections should be at maximum 5s long.

6 Implementation of Feed-forward Control

When optimal visibilities were achieved (around 96% on both detectors) and the stabilization procedure was tested and successfully performed, a line leading from the up to then unused source output to the phase modulator in the lower arm[15] of the interferometer finally could be built, containing an auxiliary detector AD and later also the voltage divider VD. This line would conduct the idler photon to AD and on detection, the detector AD would send a pulse to the phase modulator PMP, in this way performing a feed-forward control, under the condition the pulse was well timed and reached the modulator at the very moment the signal photon would have just entered it.

Timing was thus crucial for the successful accomplishment of feed-forward control. The feed-forward line was expected to induce a delay on detection which would have to be compensated for in the path of the signal photon. It was not necessary to measure this delay as results were readily available from [17]. In addition to the detector response, we had to take into account the width and shape of the TTL pulse sent by the detector AD that charges the capacitor inside the phase modulator. The feed-forward control should in the ideal case have been timed in a way so that a relatively stable (with stable voltage value) part of the pulse, behind the charging region, would be present on the modulator while the signal photon would be going through. Therefore the pulse had to be viewed and measured. The idler photon line was constructed only when all the above mentioned factors together with the propagation time in fibers and coaxial cables were considered; in a way that its optical path met the condition of simultaneous presence of the detector pulse and the signal photon on the modulator.

Finally, coincidence measurement, whose purpose was described in Section 4.2, had to be set up, using a Time-to-Amplitude Converter and Single-Channel Analyzer (TAC/SCA). TAC is capable of measuring the delay between two pulses (start and stop inputs) and generate an output pulse which is proportional to the measured time. Restricting conditions can be applied with SCA so that it analyzes the pulse only if it falls within a preset window (if the time measured falls within an interval of allowed

---

[15] The preceding text has indicated that the phase modulator used for feed-forward control was the one placed in the upper interferometer arm. However, we have realized that this was inconvenient and used the other phase modulator instead (see Section 6.2).

values), in which case it produces a countable NIM pulse. SCA also has a feature that enables it to consider a predefined delay between start and stop pulses, hence timing of the pulses measured can be done via SCA and does not have to be precise (e.g. coincidence of simultaneously generated photons can be detected at different distances from the source). In this way the TAC/SCA module can count coincident detections by evaluating the time separation of the events. Using TAC/SCA we were able work exclusively with the cases when signal and idler photons were present simultaneously in our setup, the probability of random coincidences being close to zero.

6.1 Detector Pulse Measurement

The shape and width of the pulse produced by the auxiliary detector (SPCM AQR-14FC 13610) was viewed using an oscilloscope and the following circuitry[16]:
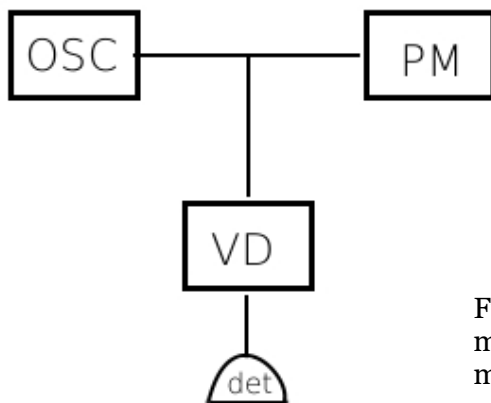

Figure 21: Circuitry scheme for detector pulse measurement. OSC – oscilloscope, PM – phase modulator, VD – voltage divider.

so the oscilloscope would show the shape of pulse arriving at PM. See Figure 22a and b for the results obtained.

We were interested in the width (full width at half maximum) of the highest part of the pulse, which was found to be around 30ns long. To ensure that we were outside the charging region, using a stable of the pulse to apply feed-forward, the delay due to the pulse inclination t_{PM} was taken for 26 ns.

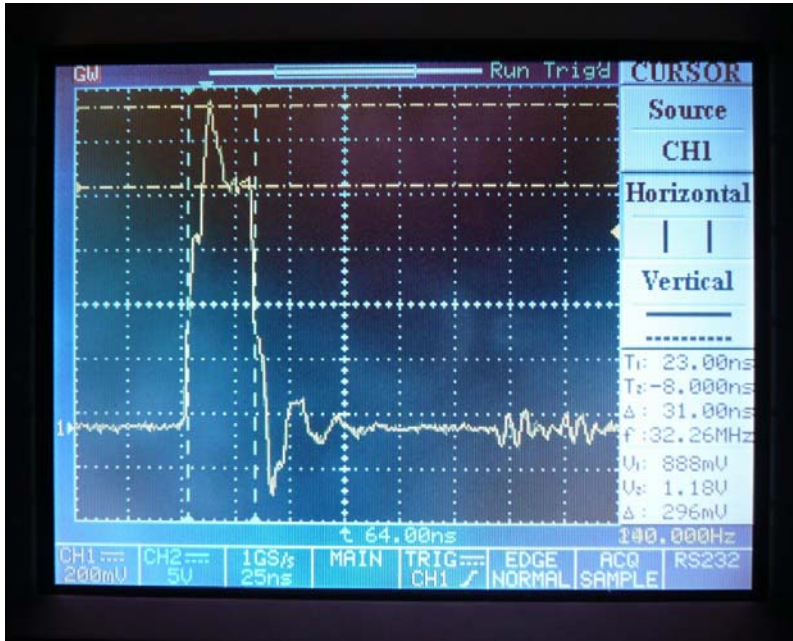[16] A scheme of the voltage divider used can be found in the Appendix.

Figure 22a: Shape of the TTL pulse from detector SPCM AQR-14FC 13610 in circuit with the phase modulator.
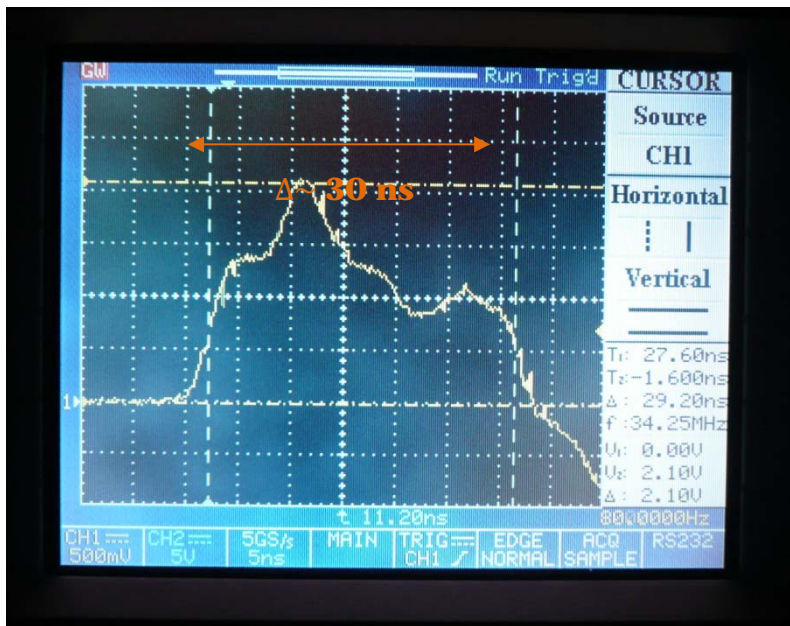

Figure 22b: TTL pulse from detector SPCM AQR-14FC 13610 zoomed in.

6.2 Evaluation of Paths Delays

As mentioned above, all delays in the signal and idler photon paths from the source to the modulator had to be evaluated for precise timing of feed-forward. The signal photon path consisted of a fiber of length a_1 going from the source to the fiber line a_2 which lead to the interferometer through the polarization controllers PC and a polarizer before the entrance fiber coupler, through the coupler into another set of polarization controllers PC 2, ending at the phase modulator PMP.

It has to be mentioned here why we have decided to use the phase modulator PMP in the lower arm of the interferometer instead of the one in the upper arm, as indicated in the preceding text and on Figure 16. During evaluations of delays we have realized that the length of the path going through the upper interferometer arm was slightly instable because of the presence of the air gap, which was observed to contract and expand by up to tens of microns and often had to be rescanned for optimal interference position. Though in terms of delay, the difference of tens of microns with respect to the propagation speed in fibers and coaxial cable should not be visible at all, we deliberately tried to avoid all instability.

Being part of the interferometer, the path length a_2 was fixed and could not be altered. If more fiber, e.g. of length X, was needed in the signal photon path, it could be added between a_2 and a_1, thus lengthening the path by X.

The idler photon optical path contained a fiber of length b_1, leading the idler from the source to the detector AD, the delay t_d due to detector response, known from [17], a coaxial cable of length b_2 connecting AD through the voltage divider VD to the phase modulator. Knowing that the index of refraction in fibers is approximately equal to $n=1.5$, so the speed of light in fiber is $v=c/n$, having measured the propagation speed[17] in coaxial cable v_k and taking into account the delay due to the modulator capacitor charging, the total delay t on the idler photon path was:

$t = b_1/v + t_d + b_2 / v_k + t_{PM}$, with

$v= c/n= 2.99792458*10^8/1.5$

$t_d=17$ ns

$v_k= 1.9764*10^8$

$t_{PM}=26$ ns

$b_1= 1540$ mm

$b_2=877$ mm,

thus $t = 55.143$ ns, which corresponded to fiber length of $v*t=11.0209$ m.

With

[17] The propagation speed in coaxial cable was measured with an oscilloscope by comparing the relative delay between two pulses for two coaxial cables of different lengths.

a_1= 3580 mm

a_2=5570 mm

we needed X=1871 mm. A fiber of appropriate length was then added between a_1 and a_2.

6.3 Coincidence Measurement

Setup for coincident detections of detectors 2 and 3 with detector AD is shown on Figure 23. Coincidences of detector 2 with AD and detector 3 with AD detections were measured on channel 3 and 4 of the counter respectively. Intensities at detector 2 needed for the stabilization procedure were measured on channel 2 of the counter. Appropriate delay had to be set on the SCA for both coincident measurements. The value was found by alternately adjusting the window position (corresponding to the delay) and narrowing the window until a maximum number of coincidences within a window of 2ns was obtained.

An average value of total coincidences was around 3200 per 10s, that is 320 per second (using results from both detectors).
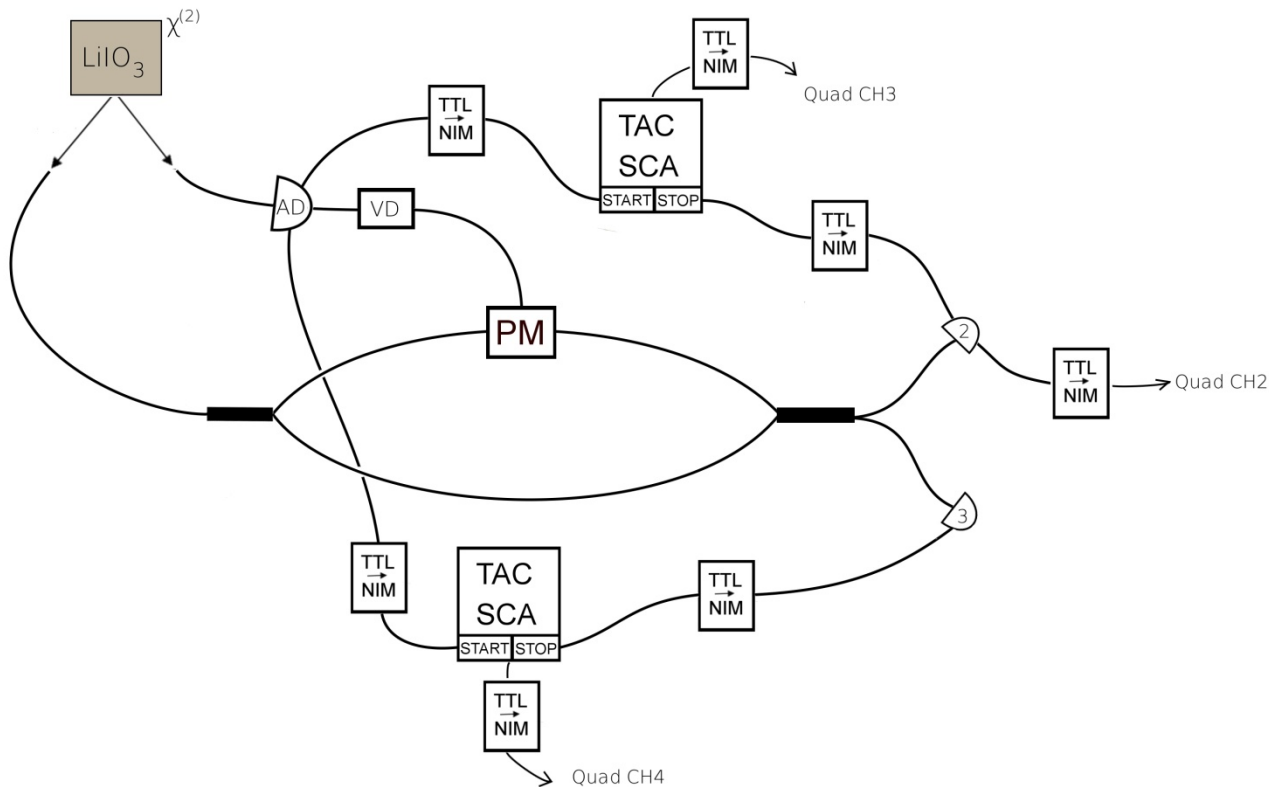

Figure 23: Coincidence measurement setup. TTL pulses from detectors had to be converted to NIM pulses which was the TAC input standard. TTL pulses produced by SCA had to be converted to NIM pulses in order to be counted by the Quad Counter.

6.4 Demonstration of Active Feed-forward

To demonstrate the effect of feed-forward control, an illustrative series of coincidence measurements was done with and without the feed-forward line connected to the phase modulator PMP, while an active stabilization process, performed via the modulator PM, maintained a minimum on one of the output detectors (detector 2). The measurement scheme was as following (see CD in Appendix for full program code of MERENI_COINCID.m):

```
measure visibility, save data
for j=1:# of measurements
   perform stabilization procedure
   set voltage to Umin
   count coincidences for 5s, save data
end
```

While a minimum was maintained on detector 2, the average value of coincidences between detector 2 and detector AD was around 20 counts per 5s, that is 4 counts per second (corresponding to a minimum) and the average value of coincidences between detector 3 and detector AD was around 1250 counts per 5s, that is around 250 counts per second (corresponding to a maximum), which yields a visibility of 97%.

The same set of measurements was done with the feed-forward line connected to the modulator PMP. It should be noted here that the presence of the feed-forward control worsens interference contrast. While fringes are being measured via PM in the upper interferometer arm, in a number of cases which corresponds to the number of coincidences a phase shift is applied in the lower arm of the interferometer by feed-forward (via PMP). With a maximum average value of 250 coincidences per second and maximum average intensity of 2000 counts per second, this would correspond to lowering the visibility by around 0.13 [18].

During a first measurement with feed-forward control, the distribution of intensity at detectors 2 and 3 was observed to be different, but not equivalent to a proper switching of maxima and minima. The resistive voltage divider (see Appendix for a scheme) in the idler photon line had to be adjusted to scale the TTL pulse, coming from detector AD, to the value of the PMP half-wave voltage, before the feed-

---

[18] Experimentally observed value.

forward control would operate as a proper switch. In order to find an output voltage value corresponding to the PMP half-wave voltage, a real-time measurement was performed while the resistances ratio inside the divider was being manipulated by means of a screw mechanism. When the proper voltage value was reached, a maximum would be read at detector 2 after it was set to a minimum following a stabilization procedure. More measurements were made with and without the feed-forward control which yielded the results shown below.

Table of average values of coincident rates per 5s[19]

Coincidences without feed-forward		Coincidences with feed-forward	
detector 2	detector 3	detector 2	detector 3
23 ± 5	1257 ± 29	1021 ± 23	43 ± 4

---

[19] Values averaged over 7 measurements.

7 Conclusion

We have successfully demonstrated the operation of feed-forward control with a fiber-optical device based on the Mach-Zehnder interferometer. After optimizing interference, we elaborated an automatic active stabilization procedure which allowed 5s-long measurements between the phase corrections, during which relatively stable minima and maxima could be maintained at the interferometer outputs. When the feed-forward control line was connected, we realized that a considerable deterioration of interference contrast occurred when intensities, not coincidences were measured; however, the stabilization procedure still worked well with low visibilities[20] (around 60%). Our delay calculations were efficacious and good timing of the control pulse was achieved; it was only necessary to adjust the voltage divider output in order to achieve a functioning feed-forward which acted as a logical switch that would replace the minimum on one of the detectors with a maximum and vice versa on the other. After all, in what concerns the timing of the pulse, there was quite a lot of tolerance in terms of paths lengths, with regard to the fact that the pulse was 30 ns wide and 5ns correspond to 1m of fiber or coaxial cable.

However, if we are to elaborate on our results and make more far-reaching conclusions, more measurements will have to be made to evaluate the stability of the feed-forward switch and its dependence on the effective part of the pulse.

To sum up the progress we have made so far with reference to the longer experimental project at the end of which we should be able to produce a functional fiber-optical implementation of a programmable single-qubit quantum gate, some useful data were obtained (half-wave voltage values, transmission losses to be expected in a similar device), effective automatic procedures (air gap scan, visibility measurements, active stabilization and others) were worked out and feed-forward control was demonstrated. All this should help the successful accomplishment of the ongoing experiment.

---

[20] The values of visibility calculated were also lowered by the fact that dark counts were not subtracted from measured counts.

REFERENCES

 [1] M. Mičuda, M. Ježek, M. Dušek, and J. Fiurášek, *Experimental realization of a programmable quantum gate,* Phys. Rev. A **78**, 062311 (2008)

[2] P. Kaye, R. Laflamme, M. Mosca, *An Introduction to Quantum Computing*, Oxford University Press, 2007

[3] D. Deutsch, *Quantum Theory, the Church-Turing Principle and the Universal Quantum Computer*, Proceedings of the Royal Society of London. Series A, Mathematical and Physical Sciences, Vol. 400, No. 1818 (Jul. 8, 1985)

[4] P. W. Shor, *Polynomial-Time Algorithms for Prime Factorization and Discrete Logarithms on a Quantum Computer*, SIAM Review, Vol. 41 (1999)

[5] Ch. Zalka, *Simulating quantum systems on a quantum computer*, Proc. R. Soc. Lond. A **454** (1998)

[6] M. Dušek, *Koncepční otázky kvantové teorie*, UP Olomouc 2002

[7] M. Hayward, *Quantum Computing and Shor's Algorithm* (senior thesis), University of Illinois

[8] E. Knill, R. Laflamme, G.J. Milburn, *A scheme for efficient quantum computation with linear optics*, Nature, Vol. 409 (Jan. 4, 2001)

[9] P. Kok, W.J. Munro, K. Nemoto, T.C. Ralph, J.P. Dowling, G.J. Milburn, *Linear optical quantum computing with photonic qubits*, Rev. Mod. Phys. **79**, 135 (2007)

[10] S. Lloyd, *Almost Any Quantum Logic Gate is Universal*, Phys. Rev. Lett. **75** (1995)

[11] T. B. Pittman, B. C. Jacobs, and J. D. Franson, *Demonstration of feed-forward control for linear optics quantum computation*, Phys. Rev. A **66** (2005)

[12] F. Sciarrino, M. Ricci, F. De Martini, R. Filip, and L. Mišta, Jr., *Realization of a Minimal Disturbance Measurement*, Phys. Rev. Lett. **96** (2006)

[13] K. Zetie, S. Adams, R. Tocknell, Phys. Educ. 35(1) (2000)

[14] B. E. A. Saleh, M. C. Teich, *Fundamentals of Photonics*, Wiley (1991)

[15] L. Bartůšková, M. Dušek, J. Fiurášek, Z. Hradil, M. Ježek, M. Mičuda, L. Slodička, *Vláknová optika na telekomunikačních vlnových délkách*, UPOL (2008)

[16] Encyclopedia of Laser Physics and Technology, http://www.rp-photonics.com

[17] L. Bartůšková, *Měření doby odezvy SPCM*, protokol ze 17.6.2008

[18] M. Dušek, *Měření půlvlnného napětí fázových modulátorů*, protokol ze 4.11.1997
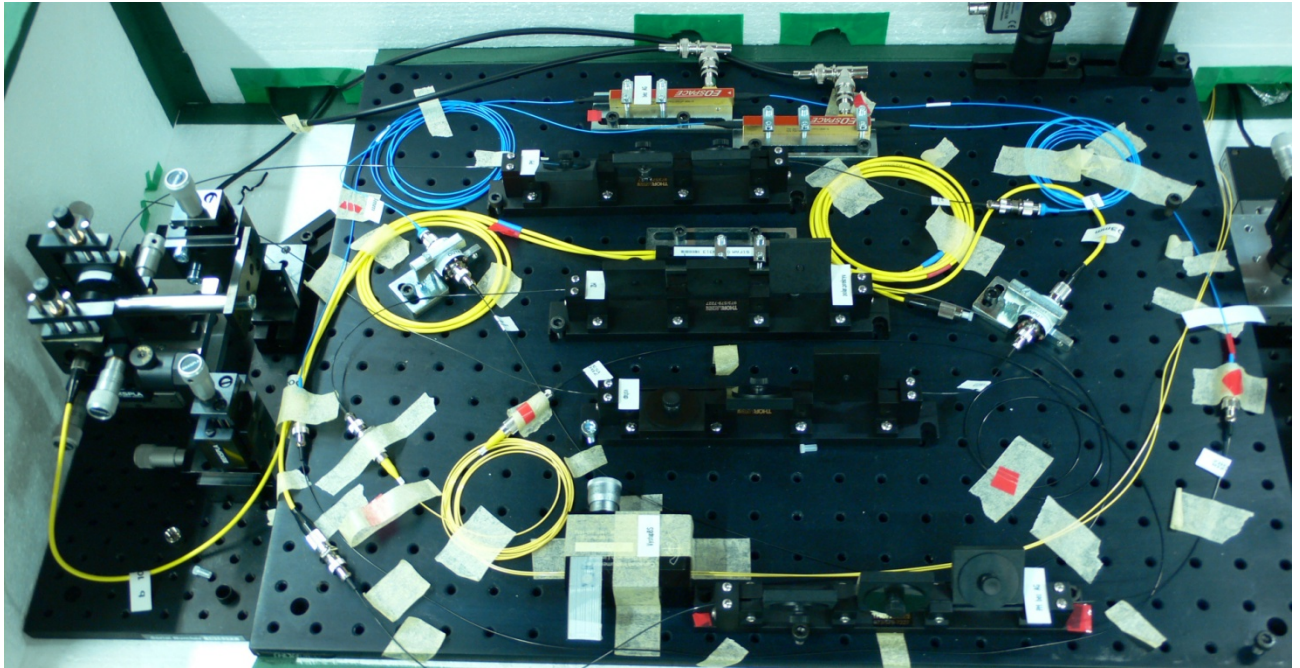
APPENDIX

A1 Setup

Figure A1: Experimental setup. The fiber Mach-Zehnder interferometer was placed in a polystyrene box for thermal isolation. The source of entangled photon pairs and detectors cannot be seen on this picture. Components in the lower interferometer arm (without air gap) are marked with red tape.

Table of typical count rates:

Counts rates for:	Counts per second
Signal photons	25 000
Idler photons	24 000
Transmission through interferometer (setup without feed-forward)	2300
Transmission through interferometer (setup employing feed-forward)	2100
Dark counts - detector 2	390
Dark counts - detector 3	320
Total coincidences	318

A2 Half-wave voltage measurements results
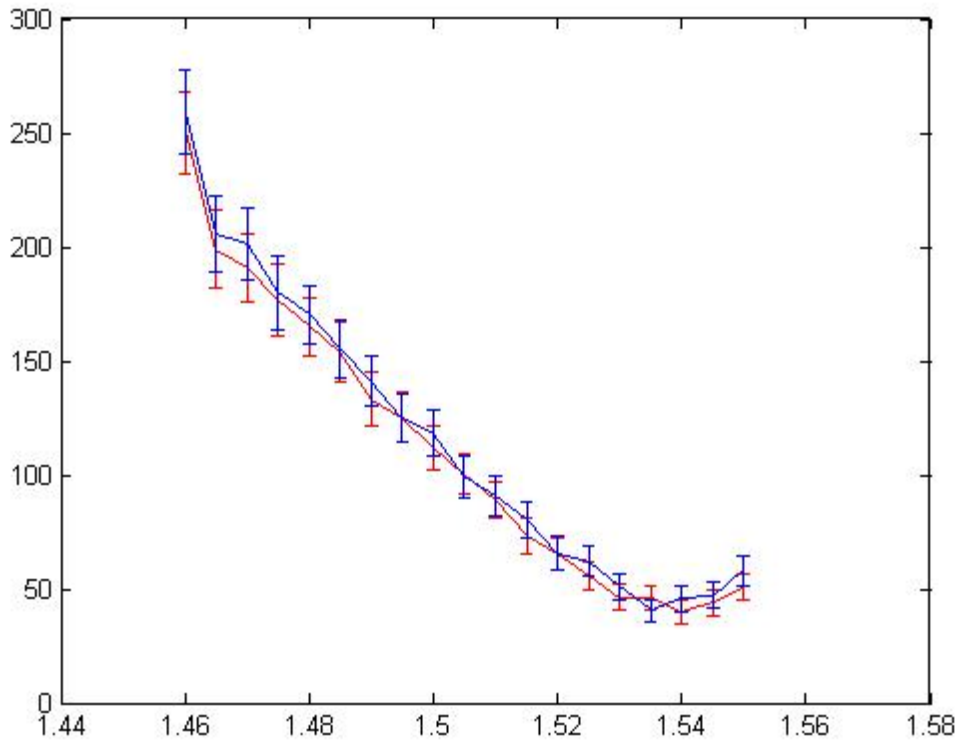
Figures A2 a and b: Results for the PMP phase modulator with an integrated polarizer, showing error of estimated mean (b).
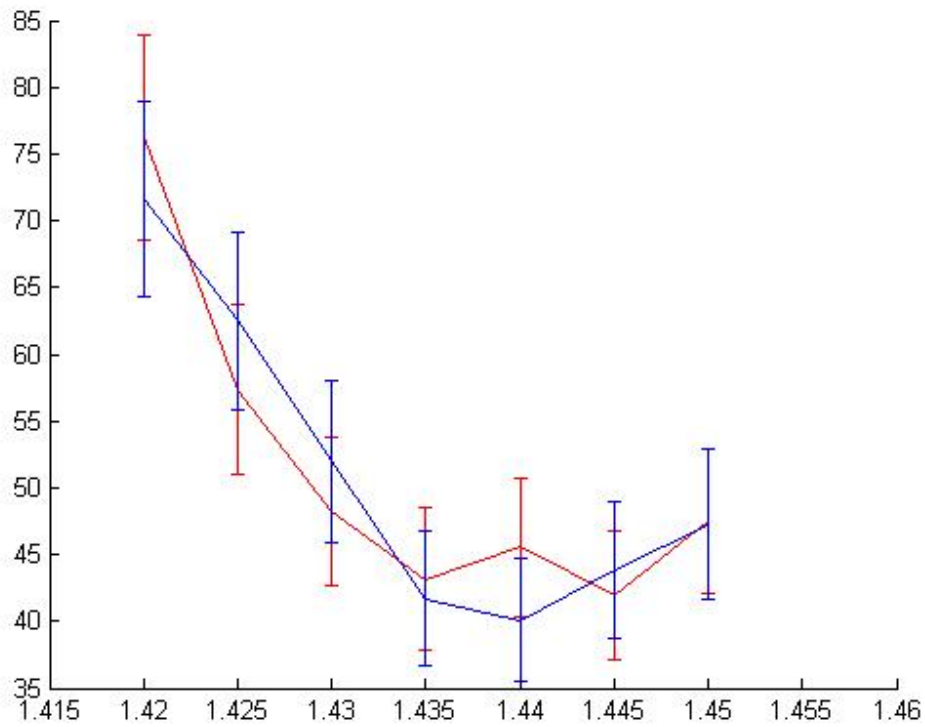
Figures A2 a and b: Results for the PM phase modulator, showing error of estimated mean (d).
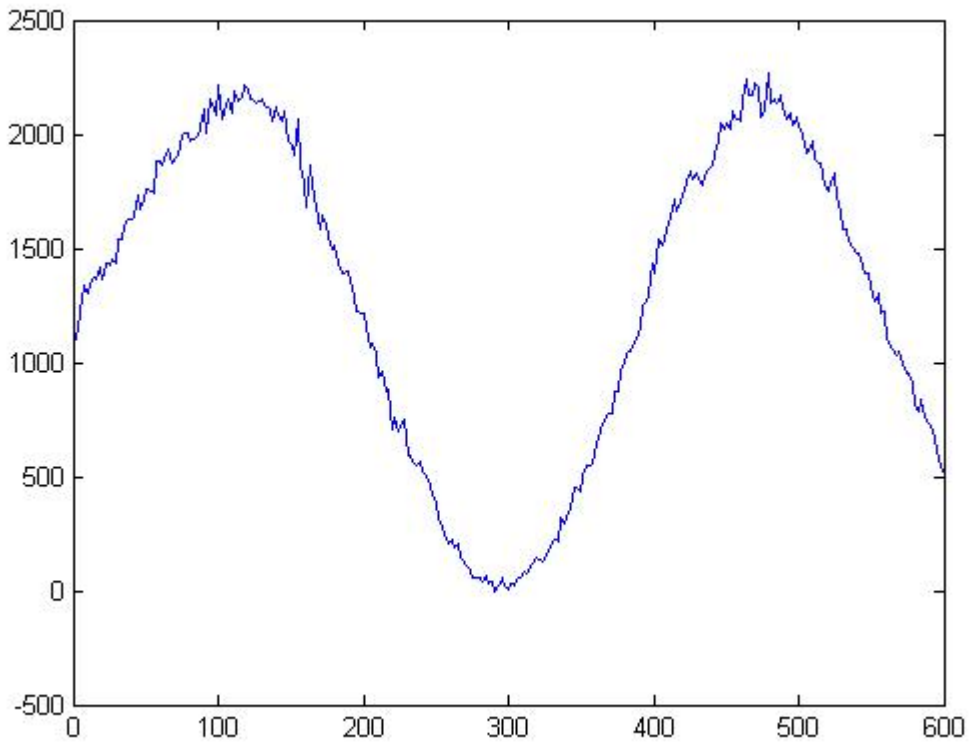
A3 Interferometer stability

Figure A3: Count rate vs. time. After a successful stabilization procedure, count rate was measured for 600s. As can be seen from the plot, the result corresponds to a phase shift of 3π / 600s approximately.
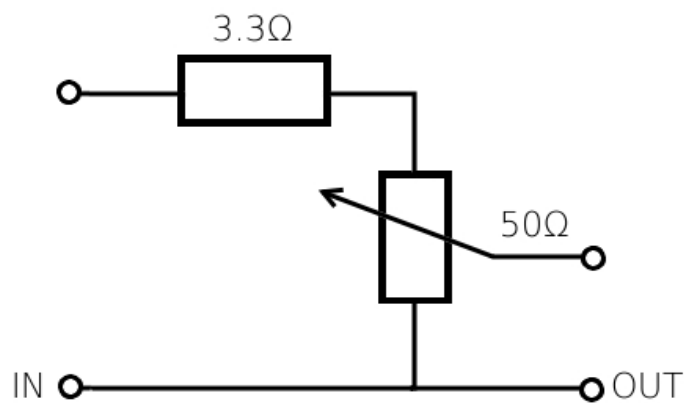
A4 Voltage divider scheme

Figure A2: Scheme of the voltage divider used for scaling of the TTL pulses.